# Size Controlled Synthesis of Transition Metal Nanoparticles for Catalytic Applications

Thesis by

Angel Tonatiuh Garcia Esparza

In Partial Fulfillment of the Requirements

For the Degree of

Master of Science

King Abdullah University of Science and Technology

Thuwal, Kingdom of Saudi Arabia

July 2011

The thesis of Angel Tonatiuh Garcia Esparza is approved by the examination committee.

Committee Chairperson: Kazuhiro Takanabe

Committee Member: Peng Wang

Committee Member: Valentin Rodionov

## ABSTRACT

Size Controlled Synthesis of Transition Metal Nanoparticles for Catalytic Applications

Angel Tonatiuh Garcia Esparza

Catalysis offers cleaner and more efficient chemical reactions for environmental scientists. More than 90% of industrial processes are performed with a catalyst involved, however research it is still required to improve the catalyst materials. The purpose of this work is to contribute with the development of catalysts synthesis with two different approaches. First, the precise size control of non-noble metals nanoparticles. Second, a new one-pot synthesis method based on a microemulsion system was developed to synthesize size-controlled metal nanoparticles in oxide supports. The one-pot method represents a simple approach to synthesize both support and immobilized nanometer-sized non-noble metal nanoparticles in the same reaction system. Narrow size distribution nickel, cobalt, iron and cobalt-nickel nanoparticles were obtained. High metal dispersions are attainable regardless the metal or support used in the synthesis. Thus, the methodology is adaptable and robust. The size-controlled supported metal nanoparticles offer the opportunity to study size effects and metal-support interactions on different catalytic reactions with different sets of metals and supports.

## ACKNOWLEDGMENTS

*"He who would learn to fly, one day must first learn to stand and walk and run and climb and dance; one cannot fly into flying" - Friedrich Nietzsche*

Every goal I pursue and every success I am able to achieve will always be because of my wife. I cannot remember life before I met her because today, she is my strength and motivation in every step I take. The study presented here is only a small step towards a bigger scientific goal, and my wife is the driving force behind my hard work and determination to contribute to science.

My parents and sister are the safety net in my existence. They are always part of my heart no matter where I am. During my career, I have only cared about making them proud. I want to thank them for supporting me regardless of what I do in my life.

I did not know Science before meeting my supervisor Kazuhiro Takanabe. Everything I know about it is because of him. He has become more than a supervisor and I look at him with respect and admiration. He accepted me and taught me that two of the most important things in science are hard work and determination to achieve our objectives. I will always be grateful to him for the rest of my life.

In our research group, we work towards a common purpose. The objective of our research will impact human society in significant dimensions and that is how my supervisor and his team showed me the beauty that is the job of a scientist. Gui-Jun Ma, Dilshad Masih, Xiaoming Liu and Xuyuan Peng helped me in every step of my research. I want to thank them for supporting me and showing me the best practices in research.

This thesis would have not been possible without the help of research scientist Dr. Dongkyu Cha. He invested his time to analyze all the samples under TEM and I want to thank him for his advice and support.

Since the beginning of my work, Paco Laveille, Sammy Ould-Chikh and Gregory Biausque were there to motivate me. They were always willing to give me advice in all aspects of inorganic synthesis.

# TABLE OF CONTENTS

## LIST OF ILLUSTRATIONS

Figure 6. XRD diffraction patterns corresponding to the 10 wt.% samples synthesized via homogeneous deposition-precipitation. Broad peaks are found in the nickel and cobalt-nickel patterns, while in the cobalt sample shows a well-crystallized phase.

Figure 7. XRD diffractograms of the amorphous samples obtained form HDP. Same codes and same legends are used as in Figure 6. The phases identified in the nickel sample are hydroxide phases of the metal. No clear crystallized phases of cobalt or mixed Co-Ni metals were found in the sample HDP-10-CoNi.

Figure 8. XRD pattern of the 10 wt.% cobalt synthesized sample. Only one clear crystallized phase is identified. The peak without identification around 67° correspond to amorphous γ-Alumina.

Figure 9. TEM image of nickel nanoparticles prepared via microemulsion method without support. Section A of the figure shows the nanoparticles for $w = 2$ with surfactant concentration of 0.5 M. Section B presents the result with $w = 10$. Both samples have the same nickel concentration of 0.17 M in the aqueous solution. The scale bar on the left figure corresponds to 2 nm and the scale bar on the right is 5 nm.

Figure 10. TEM image of a nickel particle found in a sample with a $w = 10$ and a nickel concentration of 0.85 M in the aqueous solution used in the MEM synthesis with surfactant concentration of 0.5 M.

Figure 11. Schematic representation of the results. From left to right, the samples correspond to Figure 9.A, Figure 9.B and Figure 10.

Figure 12. TEM images of 2.5 wt.% nickel nanoparticles supported on alumina. Samples A, C and D have a 2 nm scale bar in the right bottom of the figure; figure B has a 5 nm scale bar.

Figure 13. EDX energy distribution for a 2.5 wt.% $Ni/Al_2O_3$ sample with *w* = 3. Inset A represents the reference image for the EDX analysis and Inset B shows the Ni mapping with EFTEM.

Figure 14. TEM images of 0.5 wt.% nickel nanoparticles supported on alumina. Figures A, B and D have a 2 nm scale bar in the right bottom of the figure; figure C have a 5 nm scale bar.

Figure 15**.** TGA results for microemulsion samples synthesized with a 2 wt.% loading in zirconia. The y-axis represents the weight of the sample in percentage. The broken arrows indicate the percentage of weight loss during the experiment. The experiment was done under 100 ml/min of flowing air and temperature was incremented at a constant rate of 10 °C/min from RT to 800 °C.

Figure 16**.** XRD diffraction patterns obtained from 2wt.%Ni, Co, Fe and Co-Ni loaded samples in zirconia produced via microemulsion with *w* = 4.

Figure 17. Diffractograms of the XRD patterns taken from the previous figure between 34° and 52°.

Figure 18. XRD diffractograms of Ni, Co and Co-Ni samples with a 10 wt.% loading in zirconia. The code of the samples indicates the synthesis using the microemulsion method with *w* = 2 and BRIJ-30 concentration of 0.5 M. New peaks appear in the region between 35° and 50°.

Figure 19. XRD pattern between angles 36° and 44° from the previous figure. Ni and Co samples present new peaks and the corresponding phases are identified in top right corner of the figure with the proper symbol.

Figure 20. TPR profiles of the representative microemulsion samples. From top to bottom; the first pattern represents the reference of 2 wt.% $NiO/ZrO_2$ prepared by physical mixture; then, the following patterns represent Ni, Co and Co-Ni samples prepared with a 2wt.% loading in zirconia. The MEM system was designed with *w* = 4 and surfactant 0.87 M. The reduction was performed

under 20 ml/min flow of 5% $H_2$/Ar from room temperature to 800 °C with a 10 °C/min incremental rate.

Figure 21. TPR profiles representing a Ni sample compared with a Co-Ni sample. The samples were produced with the MEM method with w = 4 and with a desired 2 wt.% loading.

Figure 22. HRTEM images of representative samples synthesized from a microemulsion system. Part A shows a 2wt.% Ni/$ZrO_2$ sample with *w* = 4, the image shows one particle with the average size of 5 nm. Part shows a 2wt.% Fe/$ZrO_2$ sample with *w* = 4 and nanoparticles are observed with an average size of 2 nm. Surfactant concentration in cyclohexane is 0.87 M.

Figure 23. TEM images obtained from MEM samples. The samples were reduced for 30 min at 550 °C in a 50 ml/min pure $H_2$ flow. The figure compares the size of the particles depending on *w* and metal loading in the synthesis. The concentration of surfactant in cyclohexane on the synthesis is 0.5 M. Samples on the right have water content *w* = 2 and samples on the left have *w* = 8.

Figure 24. TEM micrograph obtained from a 10 wt.% Co-Ni/$ZrO_2$ sample synthesized using a microemulsion with surfactant concentration in cyclohexane of 0.5 M and *w* = 8. Reduction of the sample prior TEM characterization was performed at 550 °C for 30 min under 50 ml/min flow of pure $H_2$ gas. Two different nanoparticles are identified in the figure differentiated from the crystallographic pattern observed.

Figure 25. TEM images for two different samples (A and B). The samples are silica particles decorated with nickel nanoparticles. All variables are the same in the synthesis except the water volume in the system.

Figure 26. TEM consecutive images of the same observed particle. The beam was focused on different parts of the spherical silica particle. The distance shift is schematically represented in the insets of

the figures to illustrate where is the beam focus on the sphere. 2 nm nickel nanoparticles are trapped in the silica matrix.

Figure 27. TEM micrograph of the sample aged for 1 week after aqueous ammonia addition. Metal concentration was reduced 10 times in order to obtain $SM$ = 20.

# LIST OF TABLES

## I. Introduction

Environmental science and technology covers a very broad field of scientific knowledge. Environmental engineers work for the development of the tools and methodologies to analyze, remediate, eliminate, produce, purify, simulate and calculate all the relationships between human activity and nature. Scientists in the environmental field struggle to compile knowledge from many different scientific subjects and to understand natural phenomena and coalescent with artificial events.

By definition, environmental science is a multidisciplinary and interdisciplinary field covering fundamental topics of significant human concern. It is not possible to speak about environmental studies without mentioning pollution, global climate change, water scarcity, and alternative energy sources for clean energy production. Air, water and soil remediation is a popular topic to hear. Sustainability is a concept constantly mentioned and directly related with the definition of environment. Hazardous is a well-known word by the scientist of this field and how to manage unwanted human-made materials is a fundamental part of any environmental specialists. Genetics, diseases and bacteria are studied as well as the inorganic micropollutants developed by humans. This is only a part of the subjects overheard when speaking among environmental scientists and engineers.

All these environmental phenomena are based on chemical reactions. It is a key to control and tune rate, selectivity and efficiency for the reactions. Catalysts are the essential components to achieve this task. The catalyst is defined as a component that is involved in the chemical reactions to facilitate their rates, but

returns to its original state at the end of the reaction. Catalysis affects the reaction kinetics by introducing new transition states to control activity and selectivity towards target products of the reaction. Therefore, use of catalysts leads to less unwanted by-products, which are beneficial for both industry and the environment[1]. The largest application of a catalytic process used for environmental technology is the catalytic converters for treatment of toxic gases in car emissions[2]. Environmental science uses catalysis in areas like food processing, gas and liquid emissions cleanup, conversion and reuse of wastewater, catalytic use of renewable energy sources, reduction of environmental impact in many industrial processes, indoor and outdoor air quality improvement, catalytic remediation of water, air and soil resources and reduction of greenhouse gases[3]. The catalytic processes have significant impact on more than 90% of all industrial processes found in the world[4].

Many chemical reactions are catalyzed by metal surfaces. To increase the number of active sites, metal particles are dispersed on the high surface area support with high thermal and mechanical stability. The size of the metal particles can vary from few angstroms to tenths of nanometers. The small particles give rise to high surface area of the active sites, as well as unique surface facet and morphology, giving completely different catalytic activities and selectivities[5-7]. Therefore chemistry in material synthesis is desired to provide a very controlled size distribution of these metal nanoparticles.

The size of the metal particles depends upon the synthesis method utilized for producing the catalyst. Wet impregnation (WI) technique is one of the most commonly used synthesis methods to obtain supported metal catalysts for many

years[8-12]. In a general synthesis, a soluble metal salt is impregnated in an aqueous environment to the support. Synthesis of the catalysts is affected by various factors: textural properties of the support, pH and the ionic strength of the solution, which in turn influence adsorption process of the metal species[13,14]. The impregnation step is followed by drying, activation and, if necessary, passivation. The impregnation method assures the complete loading of metal introduced and is an economic and practical synthesis procedure[15]. Therefore, it has been widely adopted as reference preparation technique of supported catalysts. However, this method lacks a precise control of metal particle size.

Homogeneous deposition-precipitation (HDP) method produces highly dispersed nanoparticles with a high attainable metal loading. The metal nanoparticles are generated by the slow hydrolysis of urea, which controls the pH in the system and promotes a uniform precipitation of the metal precursors on the support[16-19]. Some of other synthesis methods found in the literature are the polyol method[20-22], sol-gel methods[23-25], microwave heating[26-29] and reduction of organometallic precursors in the presence of ligands.[30-33] These preparation methods have both merits and demerits, and are used depending on the application.

In metal nanoparticle synthesis, the microemulsion (MEM) synthesis method has advantages because it provides very precisely controllable size of nanoparticles at mild conditions. Schulman first introduced the term microemulsion in 1959.[34] The synthesis method utilizes a surfactant system composed of two immiscible liquids.[35] Two possible microemulsion systems are obtained, water-in-oil or oil-in-water. These two systems have opposite characteristics and structure. The metal

nanoparticles synthesis is often performed in the water-in-oil microemulsion[35-39], where the water is homogeneously distributed in the oil phase. The surfactant forms reverse micelles, where the nano-sized water droplets are surrounded with the surfactant molecules in the oil phase. The concentration of surfactant should be higher than the critical micellar concentration in order to form the reverse micelles. The formed micelles are used as microreactors to synthesize different types of inorganic materials like metals[30,40-46], metal oxides[47-49], sulfides[50-53], bimetallic metals[44,52,54-58] and complex ternary metal compounds[59-62]. Several key factors are involved when controlling the size: precursor concentration, water content, surfactant concentration and co-surfactant concentration. According to the literature, the most important parameter in this system is the water to surfactant molar ratio (*w*). By controlling the size of the water "droplet" in the system, one can control the size.

There are a considerable number of publications dealing with the control of the metal particle size. However, regularly the synthesized metal nanoparticles are only characterized but not utilized in any applications. The next step is then, what to do with the synthesized particles? As discussed previously, the desired structure as a catalyst is a supported form. Thus, a method for immobilizing the nanoparticles is essential to be developed.

The method found in the literature for the immobilization is as follows[36,37,42,58]. The support is directly added to the MEM containing the reduced metal particles and stirred vigorously. Then, polar solvents are used to destabilize the microemulsion system. Once the reverse micelle structure is destroyed, the

nanoparticles will adsorb on the support. The main problem found with this technique is the unavoidable aggregation of the nanoparticles and loss of the controlled size obtained originally. Consequently a better method for supporting the nanoparticles synthesized via a microemulsion is required.

Generally, fine control of the size and morphology of noble metals has been achieved (e.g. Pt, Pd, Rh, Au, Ag, etc.)[26,30,41,63,64], even in the order of only few angstroms. Limitation of availability of noble metals, however, drives to the substitution of them with ubiquitous metals (e.g. Ni, Co and Fe). It is therefore required to synthesize these ubiquitous metal nanoparticles in controlled size and morphology. Metal particles in less than 5 nm are of great interest because of their unique and distinguished nature in catalytic properties, as mentioned previously.[43,45,59] From the literature survey, it was found that there are limited numbers of reports that describe the application of the synthesized nanoparticles; especially, immobilization technique to support nanoparticles prepared via microemulsion. Most part of the literature found in nanoparticle synthesis always deals with noble metals only. It is generally accepted that size-controlled non-noble metal nanoparticles catalysts will allow the study of the sub-nanometer effects and it may be possible to get comparable performances with the ones observed with noble metal catalysts.

The objective of this study is the synthesis of non-noble metal nanoparticles (Ni, Co, Fe) with controlled size distribution, which are supported on an oxide support. The synthesis method using microemulsion system (MEM) was chosen because highly uniform size distribution nanoparticles can be produced taking an

advantage of very stable self-organized reverse micelles. The synthesis methodology should be flexible and robust to be able to produce reproducible results irrespective of support materials and nanoparticles synthesized in the microemulsion. Examination Committee Approvals page

The structure of this study is presented as follows. In chapter 3 reference catalysts are synthesized via wet impregnation and homogeneous deposition-precipitation. The microemulsion system is described in chapter 4 and size control of nickel nanoparticles without support is attempted. Non-noble metal nanoparticles (Nickel, cobalt, iron and cobalt-nickel) supported on alumina, zirconia and silica are synthesized in chapter 5. The catalysts obtained are characterized in detail to determine their structural and chemical properties. The yield of metal loading in the samples is confirmed by temperature programmed reduction (TPR) experiment. Transmission electron microscopy (TEM) micrographs of the supported metal nanoparticles are used to estimate the size of the crystals. X-ray diffraction (XRD) is utilized for identifying the phase of the supported metals. Finally, a new synthesis method is presented, which offers the production of size-controlled metal nanoparticles with narrow size distribution and the support in the same synthesis.

## II. Materials and methods

### 1. Nanoparticles synthesis

#### 1.1. Chemicals

All chemicals were obtained from Sigma-Aldrich (unless otherwise noted) and were used as received without further purification. The microemulsion three-phase system was formed with cyclohexane (≥99.8%), IGEPAL CO-520 (NP5, polyoxyethylene nonylphenyl ether) or BRIJ-30 (tetraethylene glycol dodecyl ether) surfactants (structures in Appendix A) and milli-Q water. Nickel (II) chloride hexahydrate (99.999%), cobalt (II) chloride hydrate (99.999%) and iron (II) chloride tetrahydrate (99%) were the metal precursors for MEM synthesis. Sodium borohydride (≥98.0%) was used as a reducing reagent. Organic solvents employed were ethanol (Absolute purity), methanol (CHROMASOLV ≥99.9%), acetone (≥99.5%), dichloromethane (DCM, ≥99.5%), tetrahydrofuran (THF, ≥99.9%) and 2-propanol (IPA, CHROMASOLV 99.9%). For the catalyst supports, aluminium oxide (99.7%, Sigma-Aldrich, surface area of 150 $m^2$ $g^{-1}$) and zirconium oxide (RC-100, Daiichi Kigenso Kagaku Kogyo CO., LTD.) were used. When performing one-pot synthesis of supported metal nanoparticles tetraethyl orthosilicate (TEOS, 99.999%) was used as support precursors. Nitric acid (65%) and ammonium hydroxide (28% $NH_3$ in water, ≥99.99%) were used to control pH of the aqueous solution. Urea (≥99.5%) was used as a precipitating agent in HDP methods.

The catalysts prepared by wet impregnation and homogeneous deposition-precipitation methods were synthesized using only metal nitrate precursors. For these supported catalysts only nickel (II) nitrate hexahydrate (99.999%) and cobalt (II) nitrate hexahydrate (≥98%) were used as precursors. The bimetallic system cobalt-nickel was done and for the impregnations the zirconia RC-100 support was utilized. For homogeneous deposition-precipitation the aluminum oxide obtained from Sigma-Aldrich was employed.

## 1.2. Synthesis methods

### 1.2.1. Impregnation

Wet impregnation samples were prepared with 16 ml of deionized water and the corresponding metal precursor; either nickel nitrate hexahydrate (99.999%) or cobalt nitrate hexahydrate (≥98%) was used for preparing the aqueous solutions of metal precursors. The impregnation samples used zirconium dioxide as support. Samples with 2 wt.% and 10 wt.% of metal loading were prepared. A required amount of metal nitrate was dissolved in the aqueous solution. After a couple of minutes of magnetic stirring, the zirconium oxide support was added to the solution. The mixture was kept under stirring overnight at 600 rpm. Then, the stirring speed was increased to 800 rpm and the solution was placed on a hot plate at 125°C until all water was evaporated. The sample obtained was dried in the oven at 85°C overnight and finally heat-treated in a furnace under static air at 500°C for 4 h.

### 1.2.2. Homogeneous deposition-precipitation

Homogeneous deposition-precipitation with urea was employed to prepare 2 wt.% and 10 wt.% loading on aluminium oxide support. First, milli-Q water was adjusted to pH 2 with $HNO_3$. Then, either $Ni(NO_3)_2{\cdot}6H_2O$ or $Co(NO_3)_2{\cdot}6H_2O$ was added to the aqueous solution. Alumina and 3 g of urea were added under vigorous stirring. The temperature was increased to 90°C and the solution kept under continuous stirring for 16 h. The pH was monitored with a METTLER TOLEDO Seven GO SG68 pH meter after calibration with known standards (pH = 4.01, 7.01 and 10.01). After the mentioned time the solution was cooled to room temperature, filtered and finally dried at 85 °C overnight.

### 1.2.3. Microemulsion method

Cyclohexane was used as the organic phase. The surfactants used were the commercially branded IGEPAL CO-520 and BRIJ-30. $NiCl_2{\cdot}6H_2O$, $CoCl_2{\cdot}xH_2O$ and $FeCl_2{\cdot}4H_2O$ were used as metal precursors and $NaBH_4$ was used as the reducing reagent. First, cyclohexane and the surfactant were mixed and stirred until a transparent stable emulsion was formed. Second, the aqueous solution with the metal ions was added into the cyclohexane and surfactant mixture. In a separate microemulsion solution, $NaBH_4$ was dissolved in water and added. The microemulsion containing the reducing reagent was quickly poured into the microemulsion with the metal precursors resulting in the reduction of the metal ions. Next, destabilization of the reverse micelle system with a polar organic solvent was performed. The result was the stabilization of the nanoparticles into the metal

oxide support (i.e., silica, alumina, zirconia, etc.). Then, the product was recovered either by filtration or centrifugation. Finally, the recovered catalysts were washed by ethanol several times, dried and finally thermally treated to remove completely the remaining organic compounds in the product. A schematic summary of the general procedure for obtaining a supported catalysis via the microemulsion method is presented in Figure 1.

### 1.2.4. One-pot microemulsion synthesis of supported nanoparticles

This one-pot method involves synthesis of both metal nanoparticles and support materials. The synthesis procedure for obtaining the reduced metal nanoparticles was the same as previously described. In summary, two equally composed MEMs were mixed; one containing the metal precursor and the other the reducing reagent. After the reduction took place, the alkoxide support precursor was added into the MEM system with the reduced nanoparticles. The support precursor underwent hydrolysis by the addition of required amount of aqueous ammonia. The reverse micelles were destabilized in the presence of excess water and the nanoparticles were incorporated into the matrix of the oxide. This procedure was developed as an alternative method for supporting the nanoparticles.

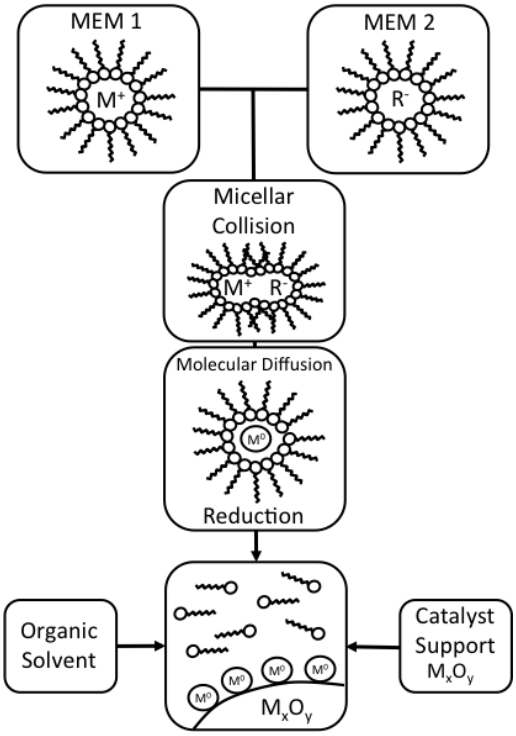


Figure 1. General schematic for the synthesis of supported metal catalysts via a microemulsion system.

## 2. Characterization methods

### 2.1. Brunauer-Emmett-Teller (BET) surface area analysis

In order to know the surface area in the catalysts and supports BET theory was used. The calculations are done by analyzing the physical adsorption of gas molecules ($N_2$) on the solid surface of the sample. Physisorption is a non-specific method for determining the total surface area of a porous material and its physical structure. Nitrogen molecules are used for the experiment where only Van der Waals forces interaction exist. The analysis procedure can be simply described as follows; first, at low pressure the inert gas molecules start adsorbing on the surface, as the pressure of the gas increases the coverage increases forming a monolayer of

gas molecules; then, multilayers will start forming while filling the smallest pores first; finally, as the pressure of nitrogen rises the sample surface will be completely covered filling all pores present. Before using BET theory the following assumptions must be made: a) Homogeneous surface, b) no lateral interactions between molecules, c) uppermost layer is in equilibrium with vapor phase, d) at saturation pressure the number of layers becomes infinite. Then following BET method the next equation can be derived

$$\frac{p}{v(p_0-p)} = \frac{1}{v_m c} + \frac{p(c-1)}{v_m c p_0} \qquad \text{E 1}$$

Where $p$ is the pressure, $v$ is the total volume adsorbed, $v_m$ represents the volume of the gas needed to form the first monolayer on the covered surface and $c$ is approximately equal to equation 2.

$$c \approx e^{\frac{E_1-E_L}{RT}} \qquad \text{E 2}$$

Where $E_1$ is the heat of adsorption of the first layer, $E_L$ is the heat of liquefaction, $R$ is the universal gas constant and $T$ is the temperature. From the experimental data an adsorption-desorption isotherm plot can be built (Isothermal plot types in Appendix B). Using this experimental information is possible to calculate the surface area using the BET equation and finally with BJH theory calculations is possible to obtain the pore volume and diameter.

The analysis was performed in a Micrometrics ASAP 2420 surface area and porosity analyzer. Standard cells for the analysis were used at all times with a known amount of sample inside. First, the samples were degassed at 200°C with a temperature incremental rate of 10°C/min for 30 min. Then, the standard nitrogen isotherm analysis at 33 K was performed.

## 2.2. Thermal gravimetric analysis (TGA)

TGA is a temperature programmed experiment where weight changes in a given sample are closely followed while varying the temperature under specific conditions. The experiment was performed in a Mettler Toledo Thermal Analyzer TGA/DSC1 Star System. The experiment conditions were set under constant flowing air at 100 ml/min starting from room temperature with a increase rate of 10°C/min until the sample reached 800°C. A known amount of sample was placed in a platinum crucible with known weight. The most important part of the instrument is the balance cell, where there is a constant measurement of the sample weight and heat flow. Regularly the experiment is used to determine different material characteristics like degradation, decomposition, corrosion, oxidation or crystallization. In this work, the experiments were used to determine the carbon content in the samples and also to estimate the required temperature for complete removable of the organic compounds remaining in the catalyst.

## 2.3. Temperature programed reduction (TPR)

Temperature programmed experiments generally are performed by varying the temperature of a sample under specific conditions. Using a thermal conductivity detector (TCD) TPR of the samples was performed with Altamira systems AMI-200ip. This system is a fully automated instrument with LabVIEW as main human interface. Before reduction experiments, all the samples were pre-treated under 30 ml/min Ar flow while increasing the temperature from room temperature to 200°C with a constant increase rate of 10°C/min and holding the final temperature for 30 min. Then, for TPR experiments a mixture of 5% $H_2$ in Ar gas was used with a constant flow of 20 ml/min. The temperature rate was 10°C/min going from room temperature to 800°C. Using LabVIEW software, the analytical area from the plots was obtained and the $H_2$ uptake from the sample was calculated. Later, using the experimental data and assuming 1:1 of $H_2$ to Metal stoichiometry the weight percentage of the metal in the catalyst sample was estimated. TPR experiment provides a clear estimation of the most efficient reduction temperature characteristic of each sample. The TCD detector will follow the gas mixture and $H_2$ will be consumed by the sample at a certain temperature, which will be recorded by the system.

## 2.4. Powder X-ray diffraction (XRD)

As the name implies, XRD is a diffraction technique used for crystalline materials. Using X-rays, as the energy source, is possible to characterize the crystallographic bulk phases of the sample, monitor kinetics of bulk transformations

and estimate the particle size. XRD experiment will show the atomic structure based on the elastic scattering of X-rays from the electron clouds of the individual atoms in the sample. The result is a specific diffraction pattern comparable to the fingerprint of the analyzed material. The diffraction pattern comes from the particular planes in the lattice calculated from Bragg's equation.

$$n\lambda = 2dsin\theta \qquad \text{E 3}$$

Which is derived from Figure B.2 in Appendix B. Where $\lambda$ represents the wavelength of the incident ray, $d$ is the plane spacing, $\theta$ is the angle between the incident waves and the planes and $n$ is an integer. Moreover, it is possible to obtain an estimation of the particle size $D$ by using the Scherrer equation

$$D = \frac{K\lambda}{\Delta(2\theta)cos\theta_0} \qquad \text{E 4}$$

Where $K$ is a constant, $\lambda$ is the x-ray wavelength, $\theta_0$ is the angle corresponding to the peak and finally $\Delta(2\theta)$ represents the area value of the full width at half maxima (FWHM) of the peak. The former equation is only valid when using a shape factor to derive the equation and only produces an average value when the particle is no smaller than 3 nm.

XRD experiments were performed on a BRUKER D8 Advance diffractometer system using a Cu Kα energy source and a Lynx Eye detector. The sample was placed

on the automated system and measurements were done at 40 kV and 40 mA from 10° to 80° 2θ angles.

## 2.5. Scanning electron microscopy (SEM)

The SEM produces images by probing the specimen with a focused high-energy electron beam that is scanned across an area of the specimen. At each point on the sample the incident electron beam loses some energy; the lost energy is converted into other forms, such as heat, emission of low-energy secondary electrons, backscattered electrons, diffracted backscattered electrons and X-ray emissions. Generally, SEM is widely used because it does not rely on transmission; it is based on surface processes and can produce (depending on the system) three-dimensional representations of the shape. Depending of the nature of the sample, it can easily characterize morphology, structure and particle size of the catalysts. Catalysts and the supports were characterized using a FEI QUANTA 3D FEG 600 electron microscope working at 15 kV. The samples were prepared by placing a small amount in carbon conductive tape on top of the sample holder.

## 2.6. Transmission electron microscopy (TEM)

On TEM the "light" source is a beam of electrons with several orders of magnitude lower wavelength than visible light, producing a resolution of a thousand times greater than a regular microscope. The electrons interact with the specimen and the image is formed from the electrons transmitted through the sample. The transmitted image is magnified and focused by using electromagnetic lenses. Finally,

the transmitted electrons hit a fluorescent screen forming the image of the specimen's "shadow"; which then can be captured with a CCD camera. The expert scientist analyzing the images can observe chemical identities, crystallographic structures, morphologies and size of the samples in sub-angstrom resolution. The TEM used for characterization is a TITAN ST transmission electron microscope from FEI operated at 300 kV. The samples were prepared suspending the sample in ethanol and dispersing it by sonication. A drop of the solution was pour into a copper-grid supported carbon film. Finally, the grid was dried at open-air prior observation.

### 2.7. Energy dispersive X-ray spectroscopy (EDX)

The EDX system is generally coupled with other techniques like the previously mentioned SEM and TEM. From the interactions of the electrons with the sample, X-ray characteristic emissions are produced and detected by an energy dispersive detector. The detector absorbs the coming X-rays by ionization, which then transforms into an electrical signal; thus, the characteristic X-rays coming from the different elements in the sample are separated and identified. The result is an energy spectrum with the characteristic peaks of the elements present in the analyzed specimen. In this way is possible to obtain an estimation of the chemical composition of the sample.

## III. Wet impregnation and homogeneous deposition-precipitation synthesis.

### 1. Introduction

Heterogeneous catalysis is the most common process found in industry for a variety of process ranging from pharmaceuticals, petrochemicals, food and environmental applications. Metal supported catalysts have been used in different process for many years and the development of this catalytic structure is very important. Synthesis of solid catalyst is an important area of research in order to be able to develop all new type of technological advances while also fulfilling all the require environmental regulations.

In industry, on of the most common methods for catalysts synthesis is the impregnation technique. In wet impregnation the objective is to fill the pores of the support structure with the active site precursor dissolved in a solution, thus the textural properties of the support is one of the most important parameters that determines the final size of the particles. Therefore, it is a difficult task to obtain a high monodispersity in the final catalyst product when using wet imporegnation.

In the synthesis process, an aqueous solution containing the metal precursor is prepared; then, the support is added with the objective of getting the adsorption of the metal precursor into the support material. The next step is to put the sample under heat treatment with static air conditions at high temperature for a determined period of time. Finally the catalyst is reduced under hydrogen flow at a

specific temperature depending on the required application reaction and specific metal active site.

Another well-known synthesis procedure is deposition-precipitation in which highly uniform and monodisperse particles can be obtained. HDP method involves the control of several parameters including the pH, the mixing process and time. For obtaining a constant and homogeneous precipitation urea is generally used as precipitating agent. The precipitation agent is used in excess in order to constantly supply $NH_4^+$ cations into the solution. In return, there is a constant control of the pH in the solution. The objective is to carefully increase the pH in order to obtain the precipitation of metal precursors into the support.

In this chapter, synthesis of supported metal catalysts was performed using WI and HDP. The catalysts obtained were characterized and used as reference materials for this work. Since the main objective of the research is to control the particle size, more investigations about these catalysts were not performed because there is no clear particle size control with these methods.

## 2. Experimental procedures

Catalysts were prepared by supporting nickel, cobalt and the bimetallic system Co-Ni in the surface of zirconia or alumina. In these syntheses the metal loading in the samples was set to 2 wt.% and 10 wt.% of the final product. A simple nomenclature will be adopted in this document in order to identify all synthesized samples. In this chapter WI and HDP samples with different loadings are described, thus the following code will apply: for example, to a 2 wt.% $Ni/ZrO_2$ sample

produced via WI the code is *WI-2-Ni*. For a sample obtained via HDP the code *HDP-10-CoNi* will correspond to a 10 wt.% Co-Ni/$Al_2O_3$ bimetallic sample.

## 2.1 Wet impregnation

Before the impregnation synthesis, the zirconium dioxide support was heat treated under static air under different temperature conditions for 15 hours. The temperatures used were 600 °C, 800 °C and 850 °C.

For the impregnation of nickel in zirconia support, 16 ml of demineralized water was used to dissolve 0.2 g of nickel nitrate hexahydrate in order to obtain a 2 wt.% loaded sample. Then, 1.96 g of zirconium dioxide was added to the aqueous solution under intense stirring. The mixture was left overnight under 600 rpm stirring. Next, the temperature was raised to 125 °C until all water was evaporated and then the product was dried overnight at 85 °C. Finally, the catalyst was treated at 500 °C under static air conditions. The obtained samples have a theoretical value of 2 wt.% and 10 wt.% of Ni supported on zirconia.

The same procedure was followed for cobalt catalyst using the according amount of cobalt nitrate precursor. In the same way, a bimetallic system of cobalt and nickel was synthesized following the described procedure. Both metal nitrate precursors were dissolved in 16 ml of Milli-Q and the ratio of metals was selected to be 1:1; in other words, 50% of nickel and 50% of cobalt are present in a 2 wt.% and 10 wt.% loaded Co-Ni sample.

2.2. Homogeneous deposition-precipitation with urea

One liter of Milli-Q water was brought to pH = 2 with the addition of of nitric acid. Once the pH of the water was carefully controlled, the aqueous solution was prepared with nickel nitrate precursor. For a 10 wt.% loaded sample, 1 g of nickel precursor was dissolved in 200 ml of water. Then, 1.8 g of alumina and 3 g of urea were added under vigorous stirring. After the addition of excess urea the temperature was increased to 90 °C and the solution was kept under this conditions for 16 h. The pH was monitored each hour. After the specified time, the pH reached a constant value of 8 and the mixture was cooled down to room temperature. Then the product was filtered using a 10 μm filtering membrane and finally dried at 85 °C overnight. The final powder was grinded and stored for further use and characterization. Nickel samples were attempted with the set loading of 2 wt.% and 10 wt.%.

Following the same specifications, cobalt samples were prepared starting from cobalt nitrate hexahydrate precursor with 2 wt.% loading and 10 wt. % loading. The same methods were adopted for the bimetallic system cobalt-nickel with a 1:1 ratio of the metals supported in the same aluminium oxide support.

Simple flow diagrams with the synthesis procedures of WI and HDP can be found in Appendix C.

3. Results

The characterization for the catalysts obtained using the WI and HDP methods was done using XRD and BET measurements. Surface area and pore

characteristics of the obtained catalyst were performed using BET calculations and BJH theory. Zirconium dioxide was selected as support for the impregnation experiments. The results of the pre-treatment of the support are shown in Table 1. Table 2 shows the structural properties of the Ni, Co and Co-Ni catalysts produced via wet impregnation and the zirconia support. Table 3 compares the textural properties of the catalysts produced by homogeneous deposition-precipitation with the alumina support used in the synthesis.

XRD measurements were performed using a Cu Kα (λ = 1.5418 Å) X-ray source under 40 kV and 40 mA. The patterns obtained for the 2 catalysts supported on Zirconia have all the characteristic peaks of the used support. From Figure 2 we can compare all the peaks corresponding to the diffraction pattern of zirconium dioxide support. In the figure, there is not clear difference between the patterns of the catalysts prepared with the loading of 2 wt.% of metal. The next figure is a more detailed description of the diffraction patterns between the 35 and 50 degrees range. Again, there is not reasonable observation of the peaks of interest.

Table 1. Textural properties changes for the Zirconia support under different temperature treatment conditions for 15 hours under static air and atmospheric pressure.

| **Temperature [°C]** | **BET Surface area [$m^2/g$]** | **BJH Desorption Average Pore Volume [$cm^3/g$]** | **Desorption Average Pore Size [Å]** |
|---|---|---|---|
| 600 | 37 | 0.22 | 230 |
| 800 | 16 | 0.10 | 213 |
| 850 | 9 | 0.05 | 200 |

Table 2. Textural properties of catalysts produced via wet impregnation.

| Sample Code | BET Surface area [$m^2/g$] | BJH Desorption Average Pore Volume [$cm^3/g$] | Desorption Average Pore Size [Å] |
|---|---|---|---|
| WI-2-Ni | 35 | 0.23 | 257 |
| WI-10-Ni | 32 | 0.19 | 234 |
| WI-2-Co | 35 | 0.22 | 245 |
| WI-10-Co | 30 | 0.18 | 231 |
| WI-2-CoNi | 35 | 0.22 | 257 |
| WI-10-CoNi | 32 | 0.19 | 232 |

Table 3. Textural properties of catalysts produced via homogeneous deposition-precipitation.

| Sample Code | BET Surface area [$m^2/g$] | BJH Desorption Average Pore Volume [$cm^3/g$] | Desorption Average Pore Size [Å] |
|---|---|---|---|
| HDP-10-Ni | 158 | 0.25 | 51 |
| HDP-10-Co | 146 | 0.25 | 54 |
| HDP-10-CoNi | 163 | 0.22 | 45 |
| $Al_2O_3$ | 158 | 0.27 | 51 |

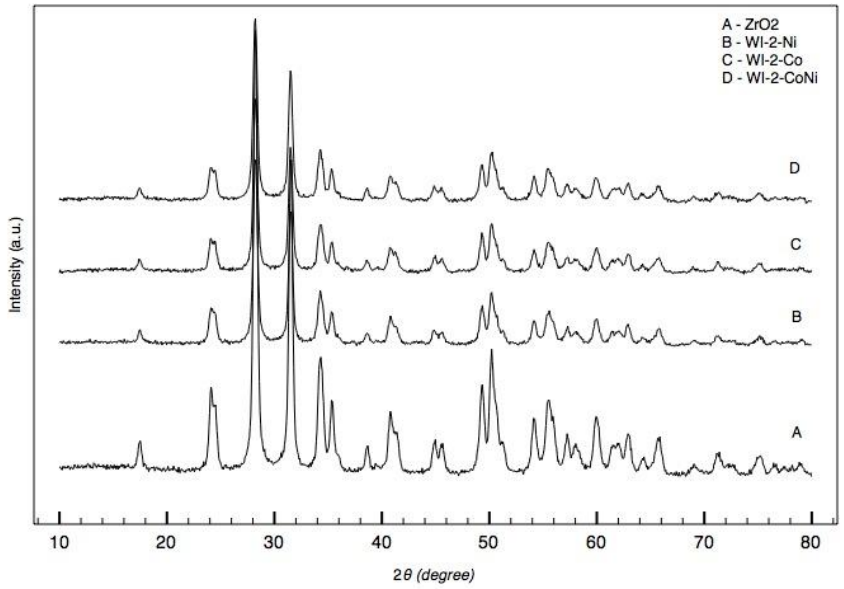


Figure 2. XRD diffraction patterns of 2wt. % metal supported on Zirconia. Ni, Co and Co-Ni catalysts appear from bottom to top after the diffraction pattern of zirconium dioxide used as reference. The legend shows the code name of the samples.

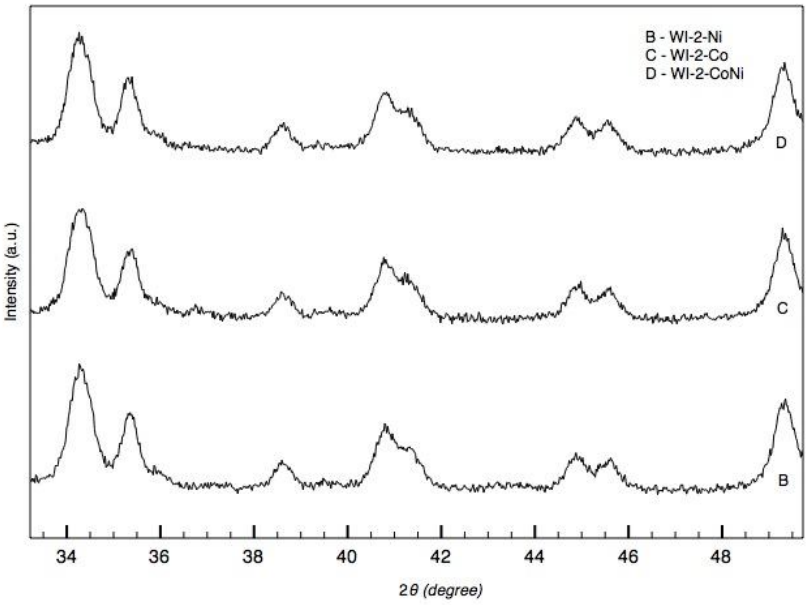


Figure 3. XRD diffraction patterns from 34 to 50 degrees in the *2θ* axis. The samples are in the same order as in the previous figure. The same legends and codes from Figure 2 are used. XRD plot for Zirconia was removed in order to provide a better analysis of the 3 samples.

Following the same line of investigation, the samples with an intended 10 wt. % loading were characterized under the same conditions and the XRD patterns are shown in Figure 4. When comparing with the reference diffractogram of zirconia, there is a clear identification of new peaks between 34° and 50° data range. Also, it is possible to observe a new peak in 19.1° which correspond to $Co_2O_3$ with a cubic structure; as pointed in the figure with the corresponding symbol. This peak can be also be barely observe in the Co-Ni sample with the same loading. A more detailed analysis of the peaks can be done in Figure 5; NiO cubic phase is found in WI-10-Ni sample. In the cobalt supported case a mixture of CoO and $Co_3O_4$, both with cubic structures, was identified. For the Co-Ni impregnated samples it is difficult to identify the phases but it is possible to observe two broad peaks, one in the $CoO{\bullet}Co_3O_4$ region around 37° and the other of NiO phase at 43.4°.

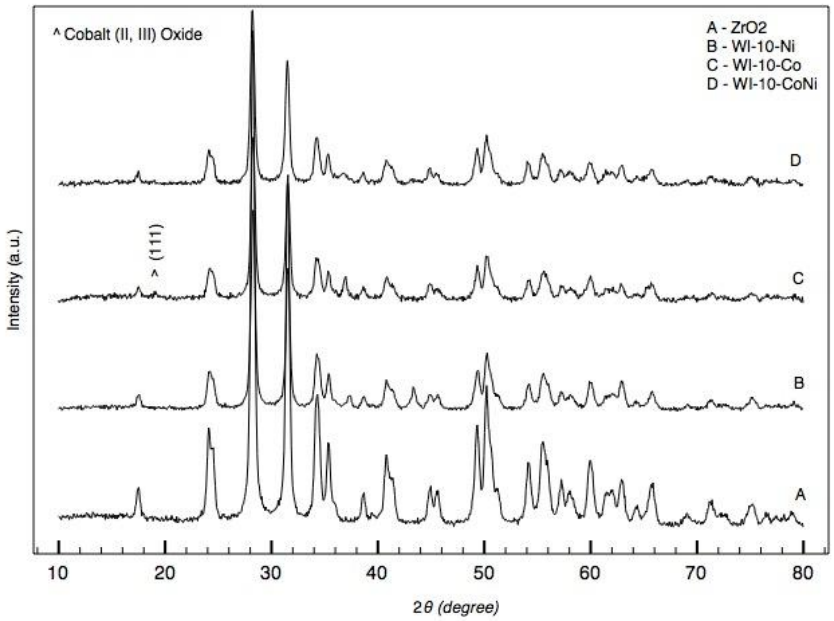


Figure 4. XRD patterns obtained from the 10 wt.% supported metal samples via wet impregnation. The code name of the samples is presented in the legend. The diffractograms of the samples are shown following the next order from the bottom to the top: Zirconium dioxide, nickel, cobalt and cobalt-nickel bimetallic system. The symbol ^ identifies one of the phases found for the cobalt supported sample.

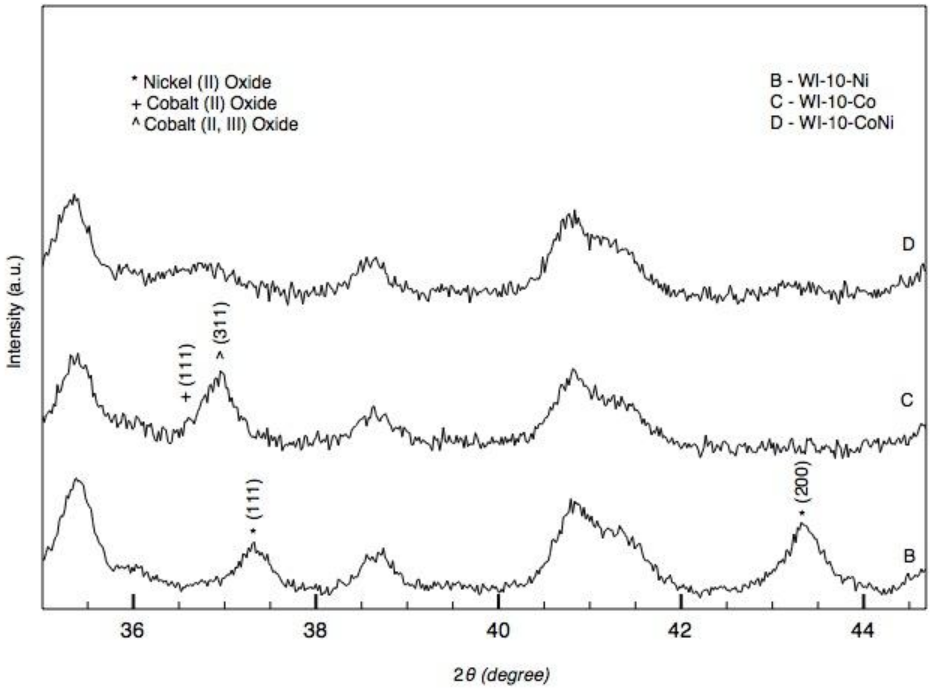


Figure 5. XRD patterns for the new peaks found in Figure 4. Ni, Co and Co-Ni samples are observed from bottom to top in their respective order. The codes and legends used in Figure 4 are the same. The symbols are shown in the legend of the top left corner of the figure representing the identified phases in the sample with their respective crystallographic planes. The rest of the peaks without proper symbol identification correspond to the zirconia support characteristic diffractogram.

The diffractograms of the samples prepared by homogeneous deposition-precipitation are shown in Figure 7 to Figure 9. The results show that the support is amorphous and not completely crystallized. In the first figure of the series it is noticeable the broad peaks found in the first three diffractograms from bottom to top. At the bottom of Figure 7 the plot for amorphous γ-Alumina is observed; although the characteristic pattern of the support corresponds, it is noticeable the broad peaks in the result. Nickel hydroxide phases differing from the broad peaks of the support were identified. The first phase is a β-nickel oxide hydroxide (NiOOH) with hexagonal system. The second phase found is the mineral known as Jamborite, which is a nickel oxide hydroxide but with stoichiometry of $Ni_5O(OH)_9$. For the sample with the metal mixture of the precursors of cobalt and nickel only a different broad peak is identified around 16°. The sample has no clear phase for any cobalt hydroxide but it conserves some characteristic peaks of the nickel sample. Finally, Figure 8 shows the crystallized phase found in the cobalt sample. The identified phase is $(Co_4Al_2(OH)_{12}CO_3(H_2O)_3)_{0.5}$ according to the PDF identification card with pattern number of PDF 01-076-3252. All peaks match to the diffractogram except the one at 67° which correspond to the amorphous γ-Alumina support. The name of the phase, as the figure states, is a hydrated cobalt aluminium carbonate hydroxide.

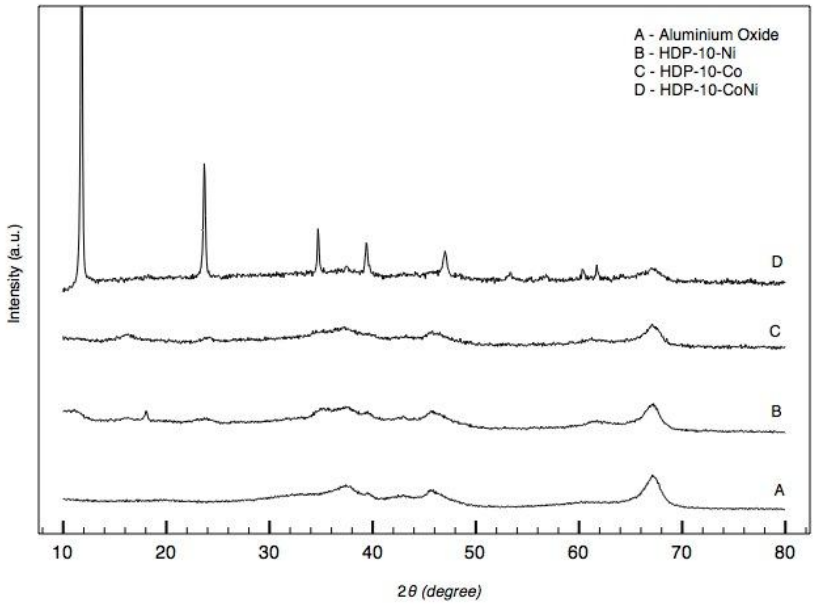


Figure 6. XRD diffraction patterns corresponding to the 10 wt.% samples synthesized via homogeneous deposition-precipitation. Broad peaks are found in the nickel and cobalt-nickel patterns, while in the cobalt sample shows a well-crystallized phase.

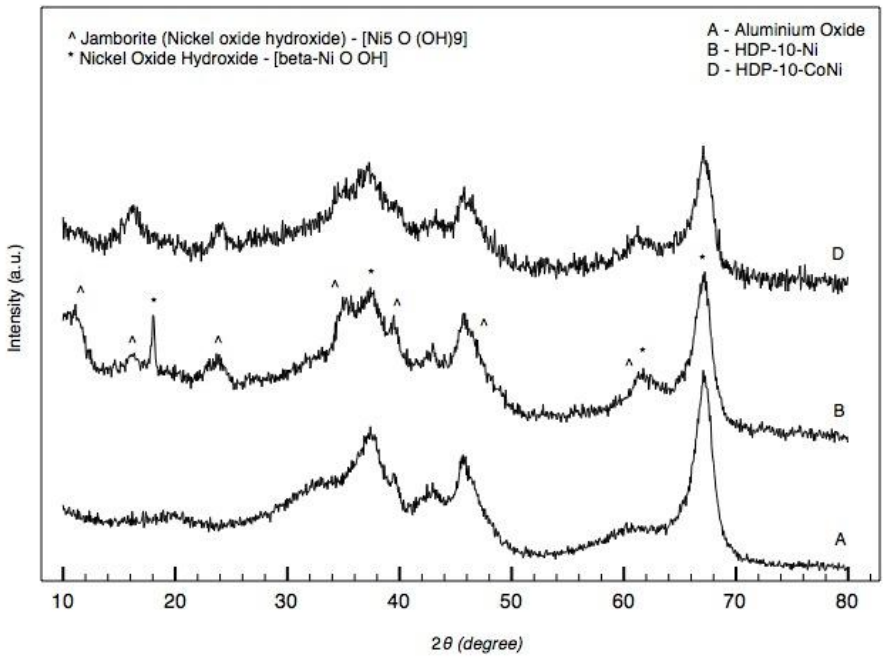


Figure 7. XRD diffractograms of the amorphous samples obtained form HDP. Same codes and same legends are used as in Figure 6. The phases identified in the nickel sample are hydroxide phases of the metal. No clear crystallized phases of cobalt or mixed Co-Ni metals were found in the sample HDP-10-CoNi. Zirconia reference diffractogram presented at the bottom of the figure.

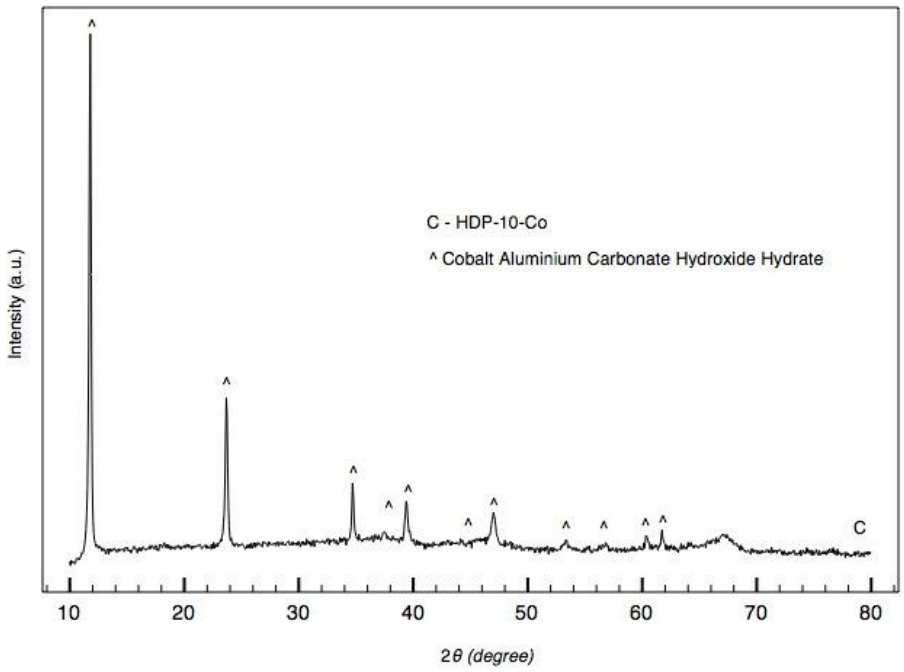


Figure 8. XRD pattern of the 10 wt.% cobalt synthesized sample. Only one clear crystallized phase is identified. The peak without identification around 67° correspond to amorphous γ-Alumina.

## 4. Discussion

In heterogeneous catalysis the selection of the proper support plays a very important role in the catalytic properties and performance of the catalyst. From the physical adsorption experiments the textural properties of the support is reflected in the samples. Zirconia sample has a low surface area (~37 $m^2/g$) compared to Alumina (~158 $m^2/g$). Thus, all the impregnated samples showed a low surface area in comparison with the homogeneous deposition-precipitation specimens. The low surface area of the zirconia sample came as a result of the temperature pre-treatment performed as shown in Table 1. It is clear that the surface area decreases as the pre-treatment temperature increases. Most of the industrial processes using heterogeneous catalysis are performed under high temperature conditions; thus

600 °C was chosen as treatment temperature for the support with the objective of improving the mechanical and thermal properties under high temperature working conditions.

In order to obtain a good dispersion of the metal in the support a large surface area is regularly required. Moreover, the performance of the catalyst is generally better due to the large dispersion of the active centers. In this research, one of the objectives is to develop a novel synthesis method with the purpose that it could be applied to different types of materials. Furthermore, one of the pre-established requirements for the synthesis methods is to be as flexible and robust as possible. With this in mind, it will be generally harder to obtain a good dispersion while using a low surface area support. Therefore, zirconium dioxide support with low surface area was employed in order to develop a general synthesis method. Furthermore, in our research group of photocatalysis it is normal to work with materials going from very low surface area (~5 $m^2/g$) to more than 100 $m^2/g$ of surface area. Therefore, a test material like the zirconia support with relative low surface area is desirable in this research. From the tables describing the results of the BET experiment is possible to notice the changes in surface area, pore volume and pore size according with the metal loading in each catalyst. As you increase the presence of the metal on the surface of the support the final value slightly decreases, which shows the presence of the metal in the sample. XRD experiments were performed in order to analyze the metal phase adsorbed on the surface of the support. In the impregnation synthesis, the samples were calcined at the end of the synthesis under 500 °C; therefore, oxide forms of the metals utilized were found to

be present in the sample. The XRD patterns were only possible to analyze when a 10 wt.% sample was employed. No clear phase identification was found in the 2 wt.% samples. The WI-10-Ni sample was found to have a bunsenite (NiO) phase with a cubic structure. The main peaks of the phase are found in 43.3° (200) and 37.4° (111). From the Scherrer equation and using FWHM it was possible to estimate the NiO particle size to be around 20±5 nm. The Zirconia support was found to have a monoclinic structure from the diffraction pattern identified. In the cobalt sample (WI-10-Co) to oxide phases were found. The most clear identifiable phase was $Co_3O_4$ with a cubic structure and main peaks found at 37° (311) and 19.1° (111) with an estimated particle size of 23±3 nm. CoO phase was also identified but most of the characteristic peaks are found to overlap with the support pattern; only one is observable at 36.6° (111) in Figure 5. It is possible that a mixture phase of $CoO•Co_3O_4$ is present in the sample because of the broad position of the peak around 37°. The bimetallic system WI-10-CoNi XRD result, also found in the mentioned figure, shows one broad peak starting around 36° and ending around 37.6°, which probably results from the combinations of the NiO phase and $CoO•Co_3O_4$ also observed in the previous samples. Then, there is another broad peak between 42.5° and 43.5° which may correspond to the NiO phase clearly identified for the monometallic nickel sample. Only a broaden line pattern was observed around 19° which will correspond to the $Co_3O_4$ phase but because it is not a clearly defined peak is not possible to assure the presence of this phase. The XRD patterns of the impregnation samples showed the presence of the oxide forms of the metals

used for the synthesis and the particle size was estimated to be around 20 nm; but monodispersity cannot be proved with XRD.

Samples with 10 wt. % loading obtained via HDP were used in the XRD experiment. The XRD results show the support to be amorphous and not completely crystallized. The broad lines observed in the diffractograms of Figure 7 are the result of a poor crystallized material; although the peaks of the XRD plots are broad is possible to observe differences between the samples. An extensive investigation and comparison of the broad peaks was performed to determine the phase found in the support. The most clear identified phase was observed in the cobalt sample (HDP-10-Co). In the cobalt sample, the identified phase was a hydrated form of cobalt aluminium carbonate hydroxide with a rhombohedral system structure probably as the result of a strong interaction of excess urea, the support and the nitrate metal precursor. For the other sample, it can be observed that they conserve the sample pattern as the support but they present additional peaks on the diffractogram. For the nickel case, β-NiOOH and $Ni_5O(OH)_9$ (Jamborite) were identified in the result. It was not possible to estimate the particle size due to the broader peaks found in the diffractogram. For the bimetallic system case, most of the peaks of the nickel hydroxide phases are conserved but there was not a clear identification of any cobalt phase due to the broaden line patterns obtained in the experiment.

# 5. Conclusions

For the homogeneous deposition-precipitation synthesis the alumina sample was selected in order to achieve higher dispersion of the metal particles and a uniform particle size distribution; which is not possible to obtain by using the impregnation technique. From the experiments it can be concluded that the HDP samples need further optimization of the synthesis process. Only the impregnation samples will be used as reference catalysts.

The impregnation technique is one of the most commonly used techniques for catalyst synthesis. From the XRD results, the particles present in the samples are in an oxide form and a further reduction step is needed in order to obtain the metallic form. The size of the particles was estimated from the Scherrer equation to be around 20 nm. Wet impregnation does not provide any means for size control.

## IV. Microemulsion method to synthesize metal nanoparticles

### 1. Introduction

Nanoparticles size is one of the most important parameters to control in the synthesis of novel metal catalysts. Scientists are in the search of understanding how to control the nanometer-sized world, in order to take advantage the quantum size effects observed under this scale.. When supported nanoparticles are used in catalysis a significant improvement in activity is generally observed due to the geometric effect exposed by nanometer-sized metal crystals.

There are different methods for controlling the structure of materials in heterogeneous catalysis. The most employed techniques for obtaining supported metal nanoparticles are the methods already reviewed in the literature survey. In this work a microemulsion system was selected from the literature as a mean to precisely control the size of the synthesized metal nanoparticles. The objective of this chapter is to show the characterization of the microemulsion system itself and to prove the ability of size control of nickel nanoparticles via the microemulsion system.

### 2. Experimental procedure

BRIJ-30 (tetraethylene glycol dodecyl ether) was used as surfactant in the MEM synthesis. The concentration on this series of experiments was 0.5 M of BRIJ-

30 in Cyclohexane. Appendix D.2 shows a flow diagram of the synthesis procedure described in this section as follows. Two equal microemulsions are produced with 55 ml of cyclohexane and 10 ml of BRIJ-30 as surfactant. Two aqueous solutions are prepared, the first one containing 0.04 g of nickel chloride and the second one with 0.06 g of sodium borohydride. The aqueous solutions, both with equal water content calculated to get $w$ = 2, are poured into each of the microemulsions respectively. After the MEM is formed with the addition of the aqueous solution containing the reactants, the MEM with the reducing reagent is rapidly mixed with the other containing the metal precursors. The reduction of the metal is optically visible by the change of color from transparent to black. After the reduction is completed, ethanol is added in the system in order to destabilize the microemulsion producing the precipitation of the product. Then, centrifugation is performed to recover the nanoparticles. Later, a cycle of washing with ethanol followed again with a centrifugation is performed. Finally, the nanoparticles are disperse with sonication in ethanol and prepared for TEM characterization with one drop of the solution into the mesh-copper grid supported on carbon foil.

For these experiments 3 characteristic samples are presented on this chapter. The synthesis parameters were designed for the investigation of size control by increasing the water content and the metal concentration in the system.

## 3. Results

The samples synthesized on this section were characterized with TEM. The images corresponding to the representative samples are shown in Figure 9 and

Figure 10. The first figure compare the size of the particles obtained using the same nickel content in the microemulsion system but varies the amount of water employed in the synthesis. The nickel concentration on the samples in Figure 9 is 0.17 M in the aqueous solution prepared with 1 ml of water. Part A of Figure 9 corresponds to a value of $w$ = 2 and Part B in the same figure was obtained with a value of $w$ = 10. In the former figure, the average particle size of the sample on the right was estimated to be around 5.6±0.2 nm; whereas the figure on the right has a rather not uniform particle size distribution, ranging from 5 to 14 nm.

The HRTEM obtained in Figure 10 shows a nickel nanoparticle found from a sample with a $w$ = 10 value but with 5 times the nickel concentration as compared with the previous samples (0.85 M in aqueous solution). The size of the particle is estimated to be around 35 nm.

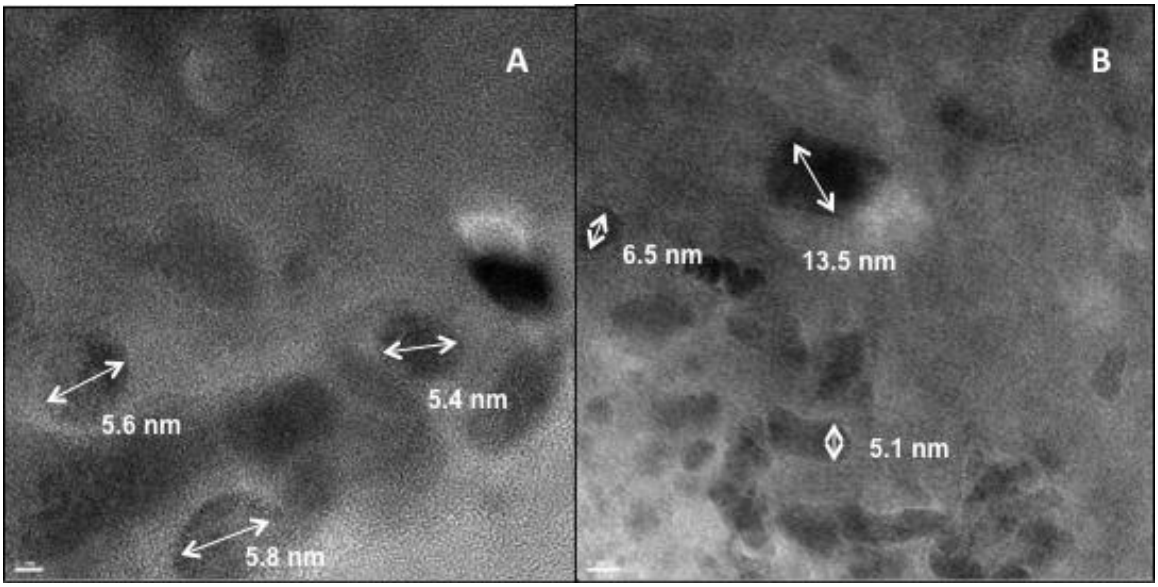


Figure 9. TEM image of nickel nanoparticles prepared via microemulsion method without support. Section A of the figure shows the nanoparticles for $w$ = 2 with surfactant concentration of 0.5 M. Section B presents the result with $w$ = 10. Both samples have the same nickel concentration of 0.17 M in the aqueous solution. The scale bar on the left figure corresponds to 2 nm and the scale bar on the right is 5 nm.

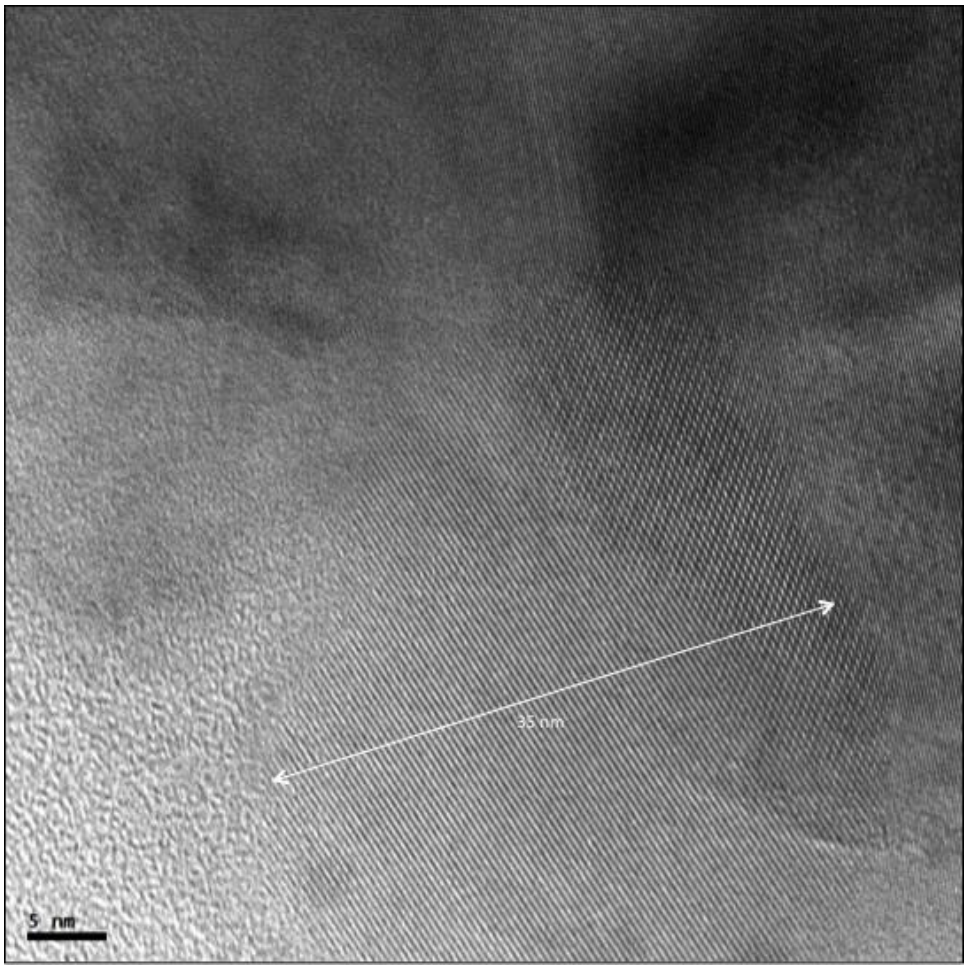


Figure 10. TEM image of a nickel particle found in a sample with a *w* = 10 and a nickel concentration of 0.85 M in the aqueous solution used in the MEM synthesis with surfactant concentration of 0.5 M.

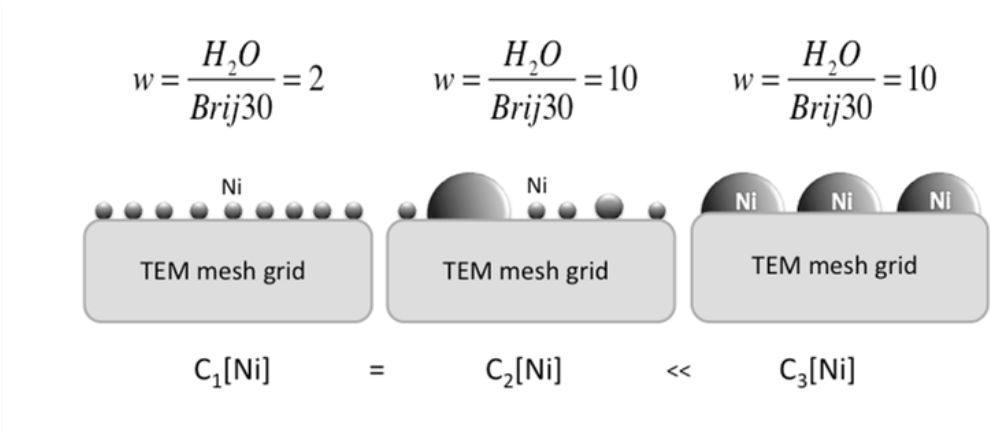


Figure 11. Schematic representation of the results. From left to right, the samples correspond to Figure 9.A, Figure 9.B and Figure 10.

## 4. Discussion and Conclusion

BRIJ-30 surfactant was used in the synthesis following the work done by Chen and co-workers (2009) where they achieve a size control of 7-30 nm.[49] From the results it is possible to observe a size control between 5 and 35 nm. The first figure compares what is the role of the metal concentration in the system. The reason is straightforward; in order to increase the particle size sufficient metal precursors are needed for particle growth. The surfactant plays the role of constraining the particle growth. Water is surrounded with the surfactant molecules stabilizing nanometer-sized microreactors. In part B of Figure 9 different size particles are observed because there is sufficient space for the particle to grow as long as the dynamic micelle collision permits reactants interchange; thus, polydisperse particles are generated in the system. From Figure 10 it was shown that once the proper concentration of the metal is present in the system the particles can grow until the final potential size, which is constraint by the surfactant and the amount of water in the system ($w$). A schematic representation of the results and the analysis already discussed is exhibit in Figure 11.

The particle size obtained with the equivalent of 1 wt.% loading of a metal onto a 1 g of support was estimated to be around 5.6 nm. While the size obtained incrementing the water content and 5 times the concentration of the metal achieved a value of approximately 35 nm.

For this research there was no control of the environmental conditions and all synthesis were performed at room temperature, atmospheric pressure conditions and open to the air. Furthermore, during this work a controlled-atmosphere sample holder was not available for TEM characterization. In Figure 10, it is possible to observe two different crystal plane orientations at the top right of the particle and at the bottom left. It was concluded from the synthesis observation that the nanoparticles are easily oxidized at room temperature conditions when exposed to air. Thus, is possible that the nanoparticle observed is a NiO nanoparticle but the crystallographic characteristics of the sample were not analyzed.

In this chapter, size control of the synthesized nickel nanoparticles was demonstrated and a more detailed understanding of the component parameters of the microemulsions was made.

## V. Supported nanoparticles synthesis from a microemulsion system

### 1. Introduction

In this chapter a suitable technique for controlling the particle size of supported metal nanoparticles is presented. A methodology for producing transition metal nanoparticles with a narrow size distribution was developed using the microemulsion method. The microemulsion system is generally formed with an organic/surfactant/water mixture in which, by controlling the composition of the phases, is possible to obtain 2 different micellar structures. If the water phase is the most abundant, a micellar system will be formed in which the surfactant molecules will surround the oil phase. In the other hand, if the oil phase is the most abundant, an inverse micellar system is produced creating micrometer sized water droplets which are used as "microreactors" for the synthesis of metal, metal oxide, alloys and other nanoparticles. Is possible to dissolve in the nanometer-sized water droplets the metal precursors ions, which later can be chemically reduced with the collisions of two equally formed microemulsions.

A general scheme for this method was already presented in Figure 1. In this section the detailed description of the synthesis of nanoparticles using MEM system will be presented. The strategy followed was to first control the size of the nanoparticles and then 3 different methods were employed to obtain supported nanoparticles. The first method was obtained directly from the literature. In a

general synthesis, once the nanoparticles are formed in the microemulsion the support is introduced into the system; then the microemulsion is destabilize in order to precipitate and reclaim the product, later the catalyst is further treated under different temperature conditions for future storage. For this method Alumina support was used in all the experiments. The second method represents a modification of the method already described in order to prevent particle aggregation. The support used for the second synthesis method is Zirconia. Finally, a novel synthesis method based on a microemulsion system was developed. The objective is to develop a robust and flexible method to obtain size controlled supported nanoparticles.

The known methods used in the literature utilize a two-step MEM process for obtaining the nanoparticles adsorbed in the support, which is similar to a wet impregnation. Thus, a one-step synthesis was developed; which in this chapter is called a one-pot synthesis of supported transition metal nanoparticles.. Nanoparticles and support synthesis happen in the same place under microemulsion-controlled conditions. Nickel metal and Silica support are used in the synthesis of this method. The third method represents a novel methodology developed, based on the microemulsion size control, to produce supported nanoparticles with high dispersity and narrow size distribution.

## 2. Experimental procedure

### 2.1 Size-controlled nickel nanoparticles supported on alumina

The reverse micellar system used in the first series of experiments of this section was formed with cyclohexane/NP5/water. Nickel nanoparticles were synthesized on these series using nickel chloride hexahydrate (99.999%) and the selected support was γ-alumina both obtained from Sigma-Aldrich. For this series of synthesis 0.5, 2.5 and 5 wt.% loaded nickel nanoparticles on alumina were attempted. The most important parameter to control in the experiment in order to control the particle size, according to the literature, is the water to surfactant molar ratio (*w*). In this work, the size of the particles is directly related to the value of *w*; although there is no mathematical correlation between this parameter and the final particle size, generally a larger value of *w* will represent the expectation to obtain a bigger particle size of the metal crystal in the synthesis. Different values of *w* were used for the experiments (*w* = 2, 3, 4, 8, 16 and 20). These values are obtained by keeping constant all the other parameters while incrementing the amount of water in the tri-phasic system. In other words, as you increase the amount of water, the size of the "microreactor" will get bigger allowing the metal nanoparticles to continue growing inside the water droplets of the microemulsion.

In a regular synthesis, two equal microemulsions are formed with 190 ml of cyclohexane mixed with 10 g of NP5. The MEMs obtained are optically transparent and stable. The amount of nickel used is directly related with the desired loading on the alumina support. In this section a 2.5 wt. % $Ni/Al_2O_3$ sample was synthesized.

The other constant parameter used in this work for the reduction of the particles was the reducing reagent-to-metal molar ratio. In order to achieve a complete and fast nucleation of the metal crystal, a constant molar ratio value of 10 was used for the synthesis. Two aqueous solutions are prepared; the first one composed of 200 mg of nickel chloride dissolved in 1.65 ml of deionized water, the second one with 320 mg of $NaBH_4$ as reducing agent dissolved in the same volume of water. For this case the calculated volume of water was used to obtain $w = 4$. Each aqueous solution prepared was poured in one of the two prepared microemulsions. Later, the microemulsion containing the reducing agent is rapidly added into the other microemulsion with the metal precursor under intense stirring. After the mixture of the two equally composed microemulsions, the reduction of the nickel ions is observed optically with the change of color from transparent to black. After the reduction is complete, 2 g of alumina was added directly to the MEM containing the reduced nanoparticles of nickel and was left under vigorous stirring overnight to promote the adsorption of the nanoparticles in the surface of the support. The next step is to destabilize the microemulsion system in order to precipitate the final product by adding 200 ml of ethanol under stirring. The product is filtered and washed several times with 50 ml of ethanol each time and finally dried overnight at 85 °C. The schematic procedure can be found in more detail on Appendix D.

The characterization done for the nanoparticles was performed using the TITAN ST TEM from FEI at 300kV coupled with EDX elemental analysis system. The dried product was dispersed in ethanol with sonication; then one drop of the dispersion was placed in a copper-grid supported carbon film and dried in open air.

## 2.2 Nickel, cobalt, iron and cobalt-nickel nanoparticles supported on zirconia

The experimental method utilized for obtaining the reduced metal nanoparticles in the microemulsion is the same as previously described. In this series of experiments the surfactant concentration in cyclohexane was to 0.87 M or 0.5 M. The metal loading was design to be 2wt.% and 10 wt.% of metal in zirconia support. The water content was varied in order to control the particle size ($w$ = 2, 4, 8). Chloride salt metal precursors were used in the synthesis. Briefly, two equally formed microemulsions are prepared; one containing the metal chloride precursor dissolved in the calculated volume of water for a specific *w,* and the other containing the reducing agent with a proportion of 1:10 respectively ($NaBH_4$). The MEM with the reducing agent is rapidly mixed with the other one and reduction of the metals is optically visible to the human eye in a matter of seconds (depending on the concentrations). At this point the nanoparticles are formed and stable inside the microemulsion system.

In order to support the nanoparticles in zirconium dioxide, a separate container was prepared with 200 ml of absolute ethanol and 2 g of zirconia dispersed on the solvent. The stable black MEM containing the metal nanoparticles is then drop by drop pour into the support solution under intense stirring. The dropping rate of the MEM was carefully control to be approximately 1.6 ml/min in all experiments. After the microemulsion is mixed with the solution support, the mixture is left stirring overnight in order to promote a better adsorption in the support. Later the product is recovered with filtration using 0.22 μm membranes and washed several times with 50 ml of ethanol each time. Then, the wet paste is dried overnight at 85 °C.

Finally, the product is calcined at 450 °C for 3 h; this last heat treatment is performed under static air conditions and was designed in order to remove the surfactant remaining in the final product. The treatment conditions were determined after the results obtained from TGA analysis. The schematic representation of the synthesis process is presented in Appendix D.3.

Characterization of the samples was performed first using TGA in order to determine the require temperature for removing the remaining carbon in the sample. TGA was done in a 75 µl platinum crucibles with a known amount of sample, the test was performed at a constant rate of 10 °C/min under 100 ml/min of flowing air.

Elemental analysis was also performed during SEM experiments in order to confirm the presence of the metals in the samples and to estimate weight percentage quantification. The samples were prepared for SEM experiment by placing a small amount of dried powder in a carbon tape fixed in a standard sample holder.

TPR experiments were used to determine the reducibility of the samples and to estimate the wt.% of the metal by assuming a 1:1 hydrogen to metal stoichiometry interaction and also assuming the complete reduction of all active sites. The method used for TPR experiments consisted in first degassing the samples under 30 ml/min Ar flow at 200 °C for 30 min. After the pre-treatment, the samples were cool down to 50 °C. The reduction was done under 20 ml/min of a 5% $H_2$/Ar gas mixture while the temperature was constantly incremented at 10 °C/min rate from 50-800 °C. Gases composition was monitored using a TCD detector at the exit of the reactor.

TEM image characterization was done for the representative samples in order to estimate particle size and to confirm if the metal was supported on zirconia. The stored samples were first reduced at 700 °C under 20 ml/min of 5% H2/Ar for 1 h. Then, the samples were dispersed in ethanol with sonication and a drop of the solution was placed on the mesh copper grid.

2.3 One-pot synthesis of supported nickel nanoparticles on silica

The synthesis of the metal nanoparticles is done following the same process as earlier discussed for the 0.87 M surfactant in cyclohexane case. The size control of the metal particles is first performed in the microemulsion reverse micelle system. Two microemulsion with 0.87 M of BRIJ-30 in 30 ml of cyclohexane are prepared. Two aqueous solutions are formed, one with the metal precursor (i.e. Nickel chloride) dissolved and the other one with $NaBH_4$. The solutions are added in each microemulsion; thus, one MEM will contain the metal precursor and the other the reducing agent. The microemulsion with $NaBH_4$ is quickly mixed with the other MEM in order to produce the reduction of $Ni^{+2}$ to nickel metal nanoparticles. The reduction is optically visible to the naked eye, the color of the MEM changes from transparent to black in a matter of seconds. Until this point, the synthesis is the same. Then, after 30 min of intense stirring and complete reduction of the metals the required support was synthesized inside the same system. The strategy was to utilize the alkoxide form of the desired support, for example, tetraethyl orthosilicate (TEOS) on these experiments. The obkective is to perform a hydrolysis of the

alkoxide with the water present in the MEM to obtain the solid support. The reaction is presented in the following equation.

$$Si(OC_2H_5)_4 + 2H_2O \rightarrow SiO_2 + C_2H_5OH \quad \text{E 5}$$

For the experiments, two TEOS/Metal (*SM*) molar ratios were used *SM* = 2 and *SM* = 20. In order to obtain a higher *SM* value, the concentration of the metal was reduced 10 times. In the synthesis, TEOS is incorporated in the MEM system with the already formed nanoparticles. Then, after 30 min 28% aqueous ammonia is added to the reaction under intense stirring and the reaction is allowed to proceed for 18 h or 1 week. Finally, in order to recover the product acetone is added dropwise to precipitate the products. The product is placed under centrifugation at 11000 rpm for 5 min and a series of washing steps are performed with 50 ml of polar solvents. After each washing, the product is dispersed again in the solvent with sonication, then centrifuge and washed again with the following solvent. The order of the washing steps is as follows; first acetone to destabilize the system, followed by THF, then DCM, 2-propanol, ethanol and finally water. The final product is dispersed in water or ethanol with sonication and stored for further use.

The parameters for controlling the particles size are the same: *w,* metal concentration and surfactant concentration. For these experiments, the water content and the *SM* ratios were varied. Only the sample with lower metal concentration and *SM* = 20 was aged for 1 week and then characterized with TEM.

For TEM characterization, the samples were already dispersed either on water or ethanol, thus a drop was directly placed in the mesh copper grid. TEM analysis was done for characterizing these series

## 3. Results

### 3.1 Size-controlled nickel nanoparticles supported on alumina

TEM image results are shown from Figure 12 to Figure 14 from this section of the work. All nanoparticles observed in the micrographs are apparently spherical particles in shape. Figure 12 shows representative samples with the same metal loading on the support while only changing *w* in the synthesis process; except from image D of the figure, in which the loading doubles in respect to the other samples. From A to D the values increase as [*w* = 2, 3, 4] and the difference between image C and D is the weight percentage of the metal present in the sample. The first impression observed from the micrographs is the agglomeration of the nanoparticles on the support. Second, all the nanoparticles show a uniform size distribution. It is also possible to have the presence of surfactant in the sample and it can be inferred from the images that the particles are still surrounded with NP5. Elemental analysis was performed in the sample and the energy distribution diagram is shown in Figure 13.

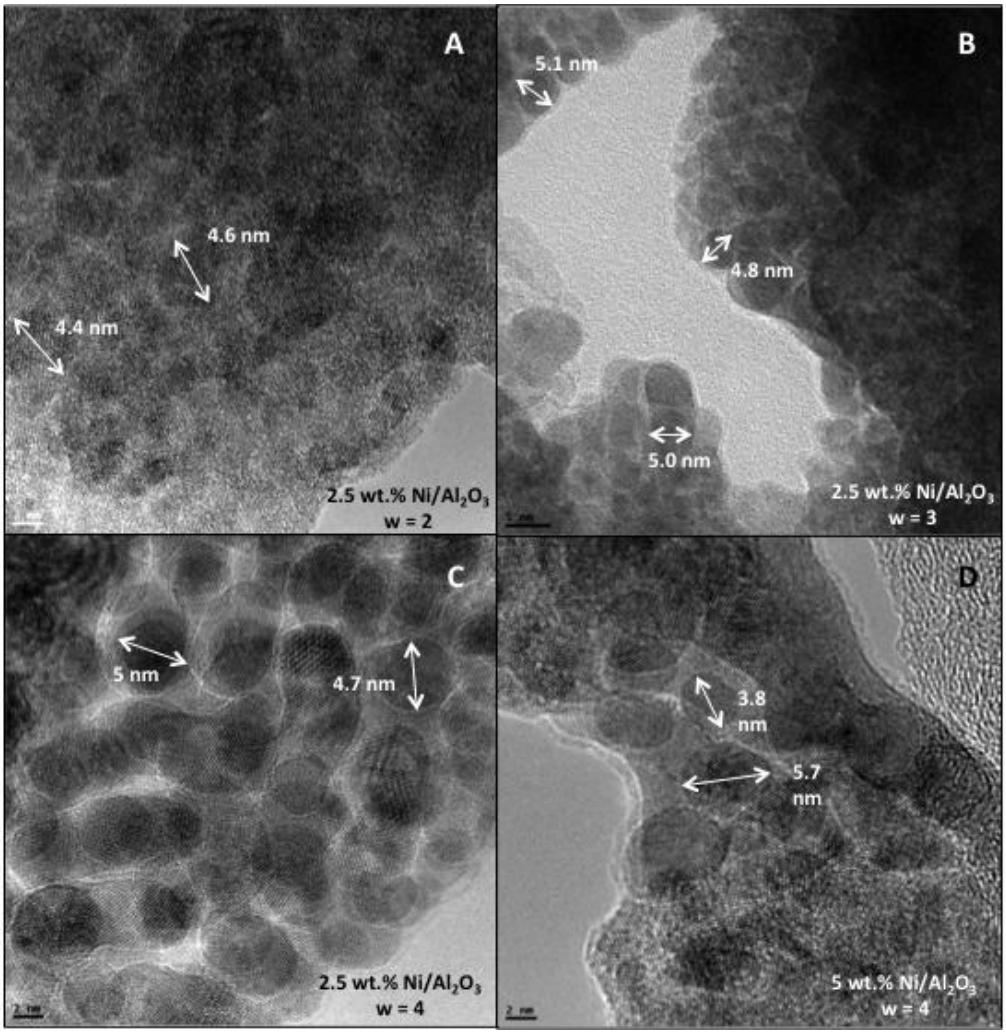


Figure 12. TEM images of 2.5 wt.% nickel nanoparticles supported on alumina. Samples A, C and D have a 2 nm scale bar in the right bottom of the figure; figure B has a 5 nm scale bar. NP5 Surfactant concentration and metal concentration were kept constant and only water content was increased for A, B and C. Sample D doubled the metal concentration and kept water and surfactant constant in respect of C.

As observed in the figure, the first peaks represent a considerable amount of carbon and oxygen present; although the sample holder is made from carbon, the intensity of the first peak could be related to the presence of the surfactant. The reference image utilized for the EDX analysis is shown in inset A with a 2.5 wt.% $Ni/Al_2O_3$ sample with $w$ = 3. The reference sample is the same image from part B of Figure 12.

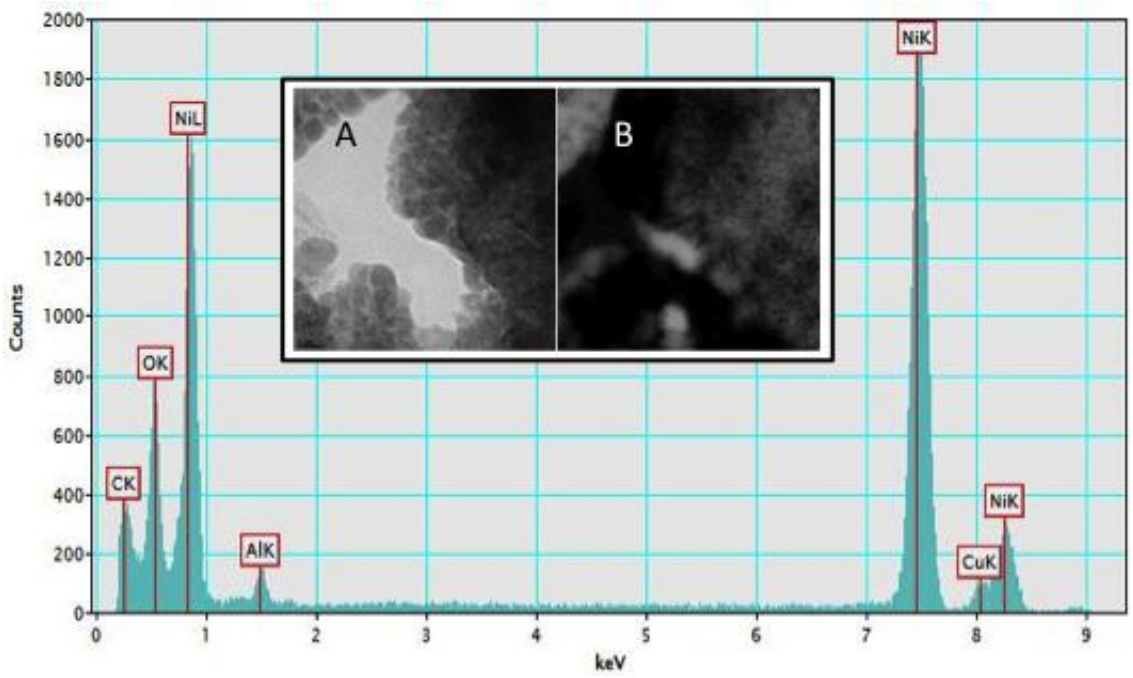


Figure 13. EDX energy distribution for a 2.5 wt.% $Ni/Al_2O_3$ sample with $w = 3$. Inset A represents the reference image for the EDX analysis and Inset B shows the Ni mapping with EFTEM.

From the energy distribution diagram it is clear the presence of nickel in the sample. Aluminium peak is also observed but the intensity is considerably lower when compared with nickel. Cupper and carbon signals may arise from the sample holder itself.

Along with EDX characterization, EFTEM technique was employed in the experiment. In this technique, the electrons with a known and specific kinetic energy are used in order to obtain an elemental map of the image. Energy-filtered TEM produces photographic elemental maps by using the inelastic scattered electrons of an EEL spectrum and a post-column with a specialized image filter (e.g.

GIF). Inset B shows the EFTEM chemical mapping identifying the presence of nickel and alumina with different contrast.

Samples with low loading of nickel in alumina were prepared following the same synthesis method already described before. The samples were calculated to have 0.5 wt. % $Ni/A_2O_3$ and the only parameter changed between the samples is the amount of water in the microemulsion; thus the values calculated are $w$ = 4, 8, 16 and 20. Figure 14 shows the TEM micrographs obtained from 4 characteristic samples of the experimental series. In contrast with previous samples, nickel nanoparticles were more difficult to observe and it was no possible to clearly identified the spherical morphology found in Figure 12.

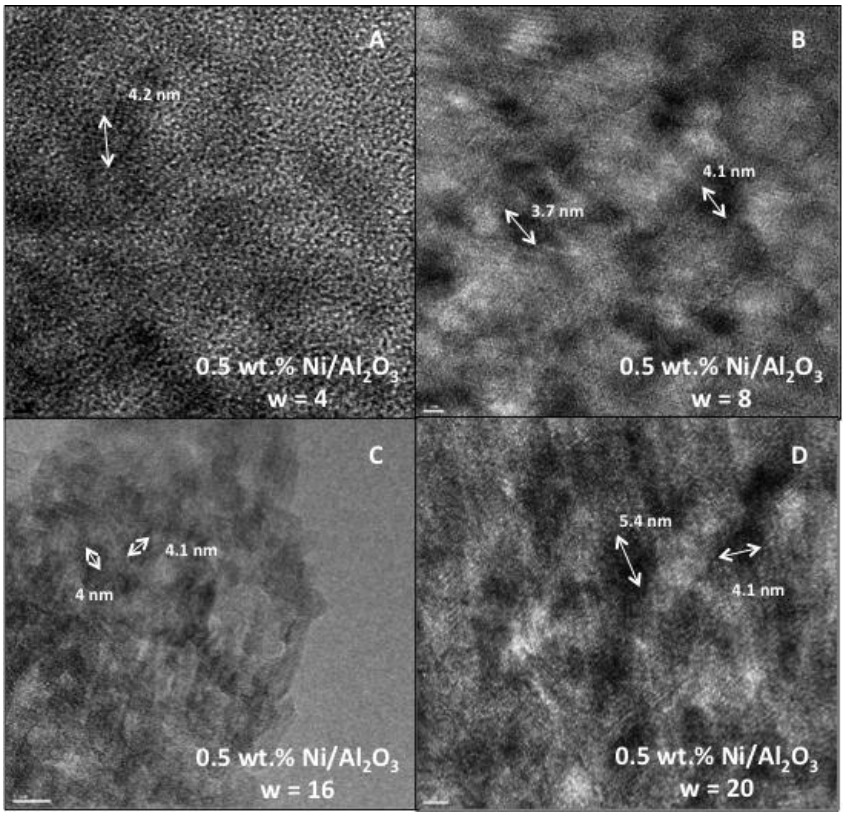


Figure 14. TEM images of 0.5 wt.% nickel nanoparticles supported on alumina. Figures A, B and D have a 2 nm scale bar in the right bottom of the figure; figure C have a 5 nm scale bar. The surfactant used was NP5.

## 3.2 Nickel, cobalt, iron and cobalt-nickel nanoparticles supported on zirconia

The synthesis conditions and methods used are the same. The difference is the surfactant concentration in the microemulsion system. The first series of experiments on this section was synthesized with 0.87 M concentration of surfactant in cyclohexane. The second series was synthesized with 0.5 M concentration of surfactant in the same solvent. The results will be used for comparison purposes and to understand the role of surfactant as stabilizer of the particles preventing them to grow further after MEM synthesis.

Thermal gravimetric analysis was done on the samples in order to determine the carbon content of the samples after the surfactant mediated synthesis and later, design the proper calcination temperature for complete removal of the remaining carbon. Figure 15 shows the results of the experiment for the Ni, Fe, Co and Co-Ni samples synthesized with 2 wt.% loading in zirconia. The x-axis represents the temperature increment from room temperature to 800 °C under flowing air at 100ml/min. The automated furnace has tow different sensors, the first one measuring the weight of the specimen and the other one the heat flow changes during the experiment. The y-axis represents the weight loss in total percentage of the original know weight in the sample.

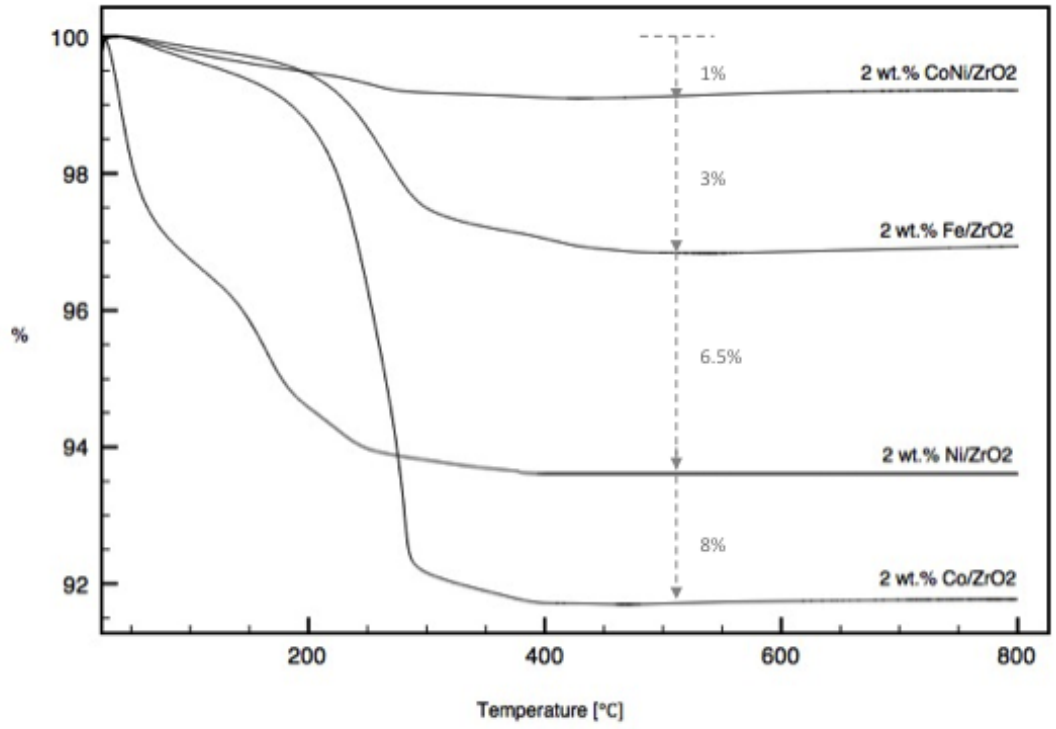


Figure 15. TGA results for microemulsion samples synthesized with a 2 wt.% loading in zirconia. The y-axis represents the weight of the sample in percentage. The broken arrows indicate the percentage of weight loss during the experiment. The experiment was done under 100 ml/min of flowing air and temperature was incremented at a constant rate of 10 °C/min from RT to 800 °C.

XRD diffractograms were recorded with a BRUKER diffractometer with a Cu Kα x-ray source. Figure 16 and Figure 17 show the obtained pattern for the representative samples of 2 wt.% metal loaded in the support. The former figure compare the support diffraction pattern to the samples, while the later shows a detailed analysis of the samples where, generally, the characteristic peaks of Ni and Co are found (i.e. between 34° and 52°). The results are similar to those found for the wet impregnation synthesis. In samples with 2 wt.% loading is not possible to easily identify the expected metal phases. The same representation and comparison is then made for the 10wt.% loaded samples in the following figures. Figure 18

compares the samples with the characteristic pattern of monoclinic zirconia; later Figure 19 illustrates the identified phases of nickel (II) oxide and cobalt (II, III) oxide. In the other hand, it is not clear the identification of the same phases in the Co-Ni bimetallic sample; with careful analysis of the diffractogram of the bimetallic sample it is possible to notice broad peaks located in the same position as the peaks of the identified phases of nickel oxide and cobalt oxide in the other samples. The intensity of the peaks corresponding to the identified phases in the sample is relatively low; thus, it was not possible to use Scherrer's equation for calculating the particle size using FWHM.

SEM images were recorded with the interest of using the coupled elemental analysis tool on the apparatus. The SEM figures showed the morphology of the zirconia support. EDS energy maps were obtained for the representative samples of Ni, Co and Co-Ni with a corresponding loading of 2 wt.% and with $w = 4$. SEM images and EDX energy maps are shown in Appendix E.1.

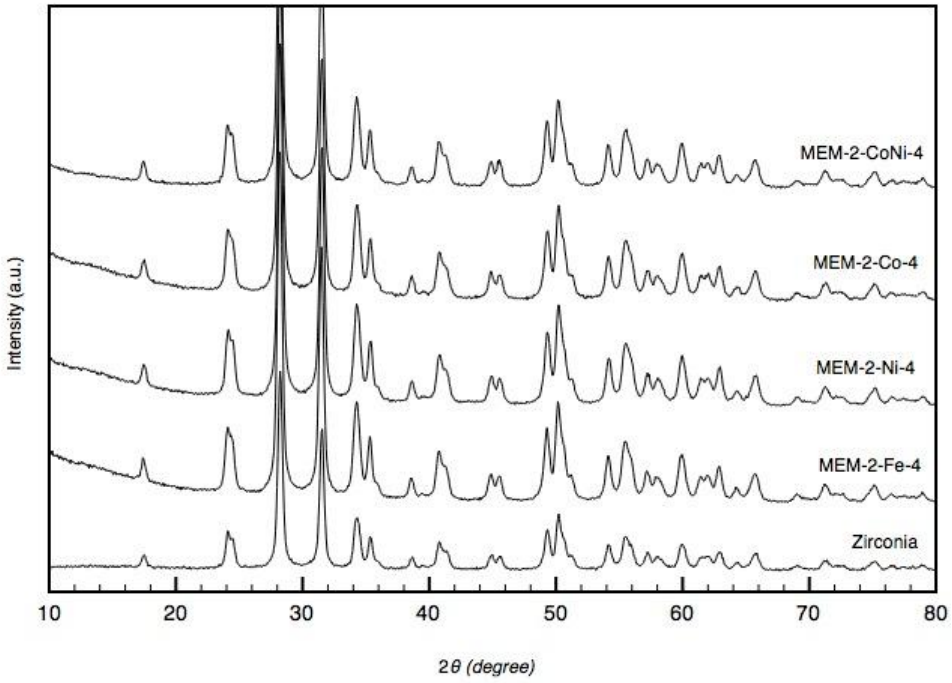


Figure 16. XRD diffraction patterns obtained from 2wt.%Ni, Co, Fe and Co-Ni loaded samples in zirconia produced via microemulsion with $w$ = 4. The surfactant used is BRIJ-30 with a concentration of 0.87 M.

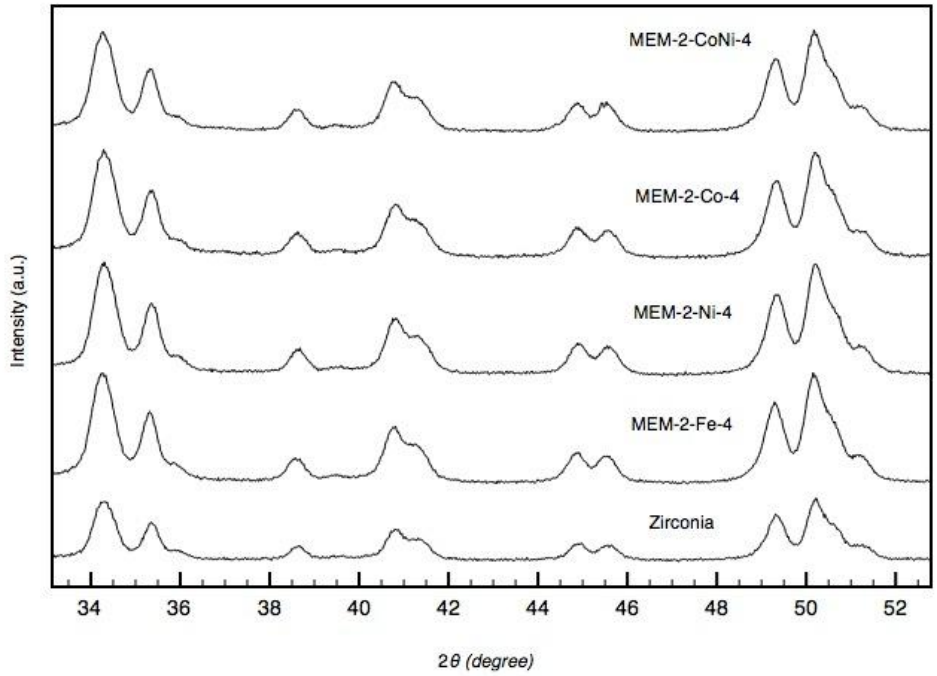


Figure 17. Diffractograms of the XRD patterns taken from the previous figure between 34° and 52°.

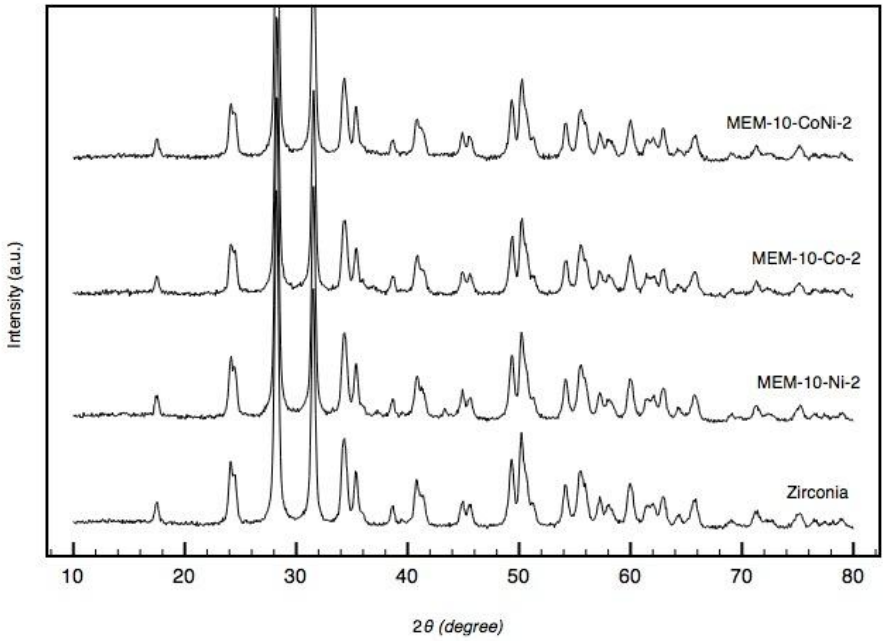


Figure 18. XRD diffractograms of Ni, Co and Co-Ni samples with a 10 wt.% loading in zirconia. The code of the samples indicates the synthesis using the microemulsion method with $w$ = 2 and BRIJ-30 concentration of 0.5 M. New peaks appear in the region between 35° and 50°.

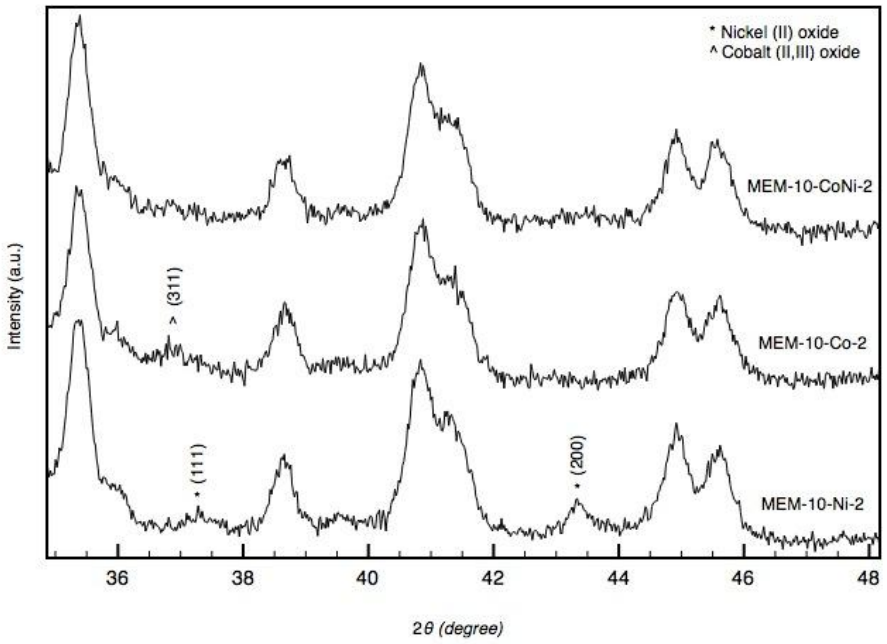


Figure 19. XRD pattern between angles 36° and 44° from the previous figure. Ni and Co samples present new peaks and the corresponding phases are identified in top right corner of the figure with the proper symbol.

TPR profiles were recorded with the reduction of a known amount of sample under 20 ml/min of 5% $H_2$/Ar gas flow. The temperature was incremented from 50 °C to 800 °C with a constant rate of 10 °C/min. TPR experiments were also performed on reference samples under the same experimental conditions. Reference samples were prepared with 2 wt.%, 6 wt.% and 10 wt.% commercially available NiO loaded in zirconium dioxide support. The components were physically mixed and grinded for 15 min. TPR results for the reference samples and calculations for obtaining the calibration equations are presented on Appendix E.2 and E.3. In Figure 20 and Figure 21 the TPR profiles obtained from 2wt.% Ni, Co and Co-Ni samples are presented in the respective order from top to bottom. The first profile was obtained from the physically mixed reference sample of 2wt.% NiO-$ZrO_2$ and shows that the reduction of NiO to $Ni^{(0)}$ starts little later than 300 °C and total reduction of the sample occurs around 450°C. Next, the synthesized nickel supported sample with the MEM method is observed to start the reduction of the nanoparticles around 350°C. Cobalt sample shows the presence of 2 reduction peaks or reduction steps; the first peak starts at 350°C and the second at 500°C. The complete reduction to $Co^{(0)}$ nanoparticles ends around 700°C. The bimetallic synthesized sample of Co-Ni nanoparticles shows 3 peaks in the profile; the first reduction peak starts few degrees after 250°C, the second reduction peak starts around 350°C and the last one at 500°C. The complete reduction of the metals present in the sample is observed around 700°C; moreover, the last peak is largely broad, thus it can be assume that most of the nanoparticles are reduced below 650°C.

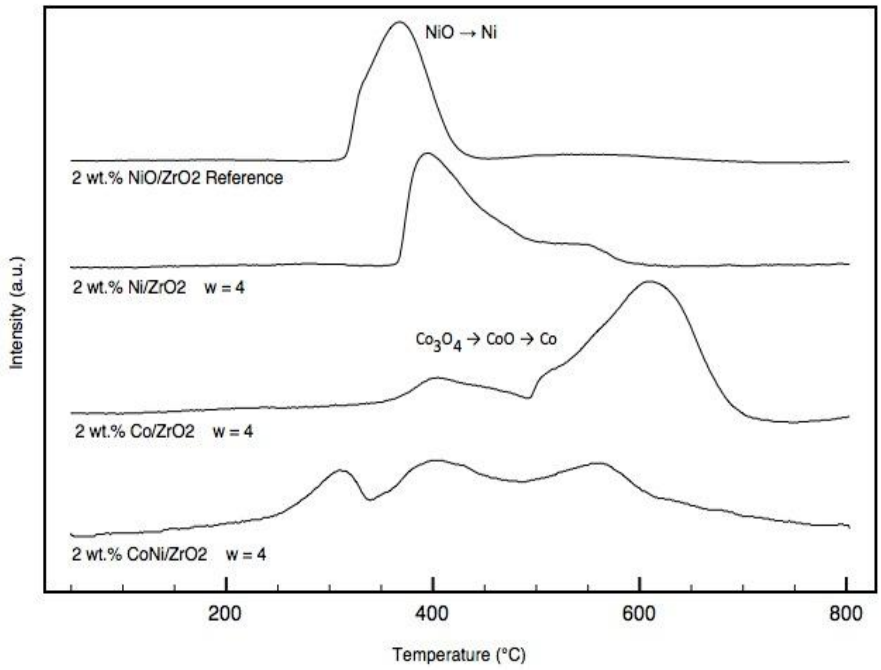


Figure 20. TPR profiles of the representative microemulsion samples. From top to bottom; the first pattern represents the reference of 2 wt.% $NiO/ZrO_2$ prepared by physical mixture; then, the following patterns represent Ni, Co and Co-Ni samples prepared with a 2wt.% loading in zirconia. The MEM system was designed with $w$ = 4 and surfactant 0.87 M. The reduction was performed under 20 ml/min flow of 5% $H_2$/Ar from room temperature to 800 °C with a 10 °C/min incremental rate.

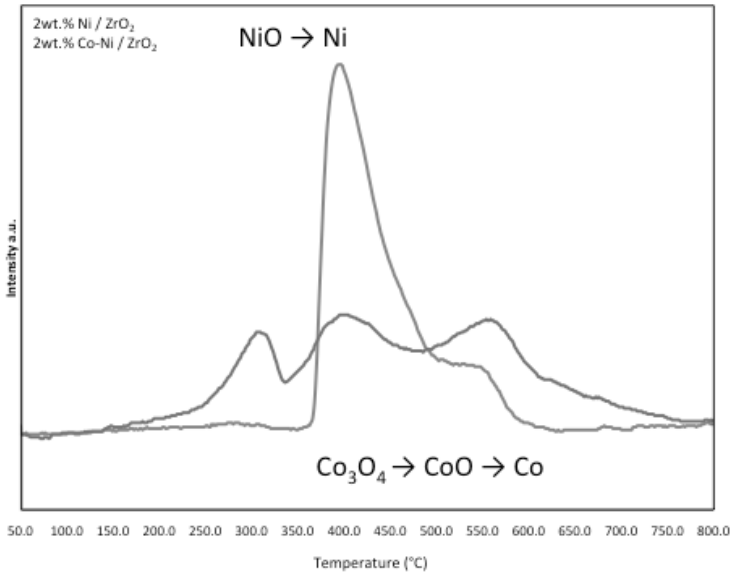


Figure 21. TPR profiles representing a Ni sample compared with a Co-Ni sample. The samples were produced with the MEM method with w = 4 and with a desired 2 wt.% loading. The profiles were taken directly from the previous figure.

TEM images were obtained for both of the experiment series synthesized on this part of the research. Representative samples using 0.87 M concentration of surfactant were characterized under the microscope. The samples were prepared as previously described. Dried powders were suspended in ethanol and dispersed with sonication. Later one drop was placed in the cupper grid sample holder and under 300 kV TEM images were captured. There was no clear identification of nanoparticles in the Co and Co-Ni with a 2 wt.% loading on zirconia. EDX were recorded and expected elements were present on the results, but samples were challenging to characterize. The water content was adjusted to $w$ = 4 for all the representative specimens. High-resolution TEM images were obtained from nickel and iron samples. Part A of Figure 22 shows supported nanoparticles with mean size of 5 nm, while part B confirms Fe nanoparticles of size of 2 nm.

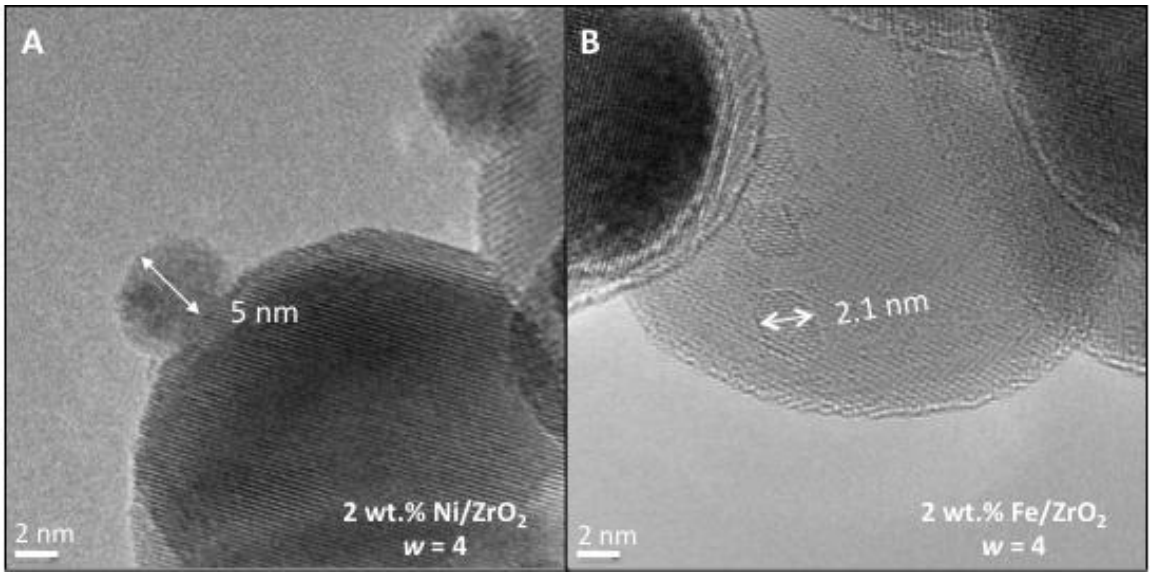


Figure 22. HRTEM images of representative samples synthesized from a microemulsion system. Part A shows a 2wt.% $Ni/ZrO_2$ sample with $w$ = 4, the image shows one particle with the average size of 5 nm. Part shows a 2wt.% $Fe/ZrO_2$ sample with $w$ = 4 and nanoparticles are observed with an average size of 2 nm. Surfactant concentration in cyclohexane is 0.87 M. Reduction of the sample prior TEM characterization was performed at 700 °C for 30 min under 5% 20 ml/min flow of H2/Ar gas mixture.

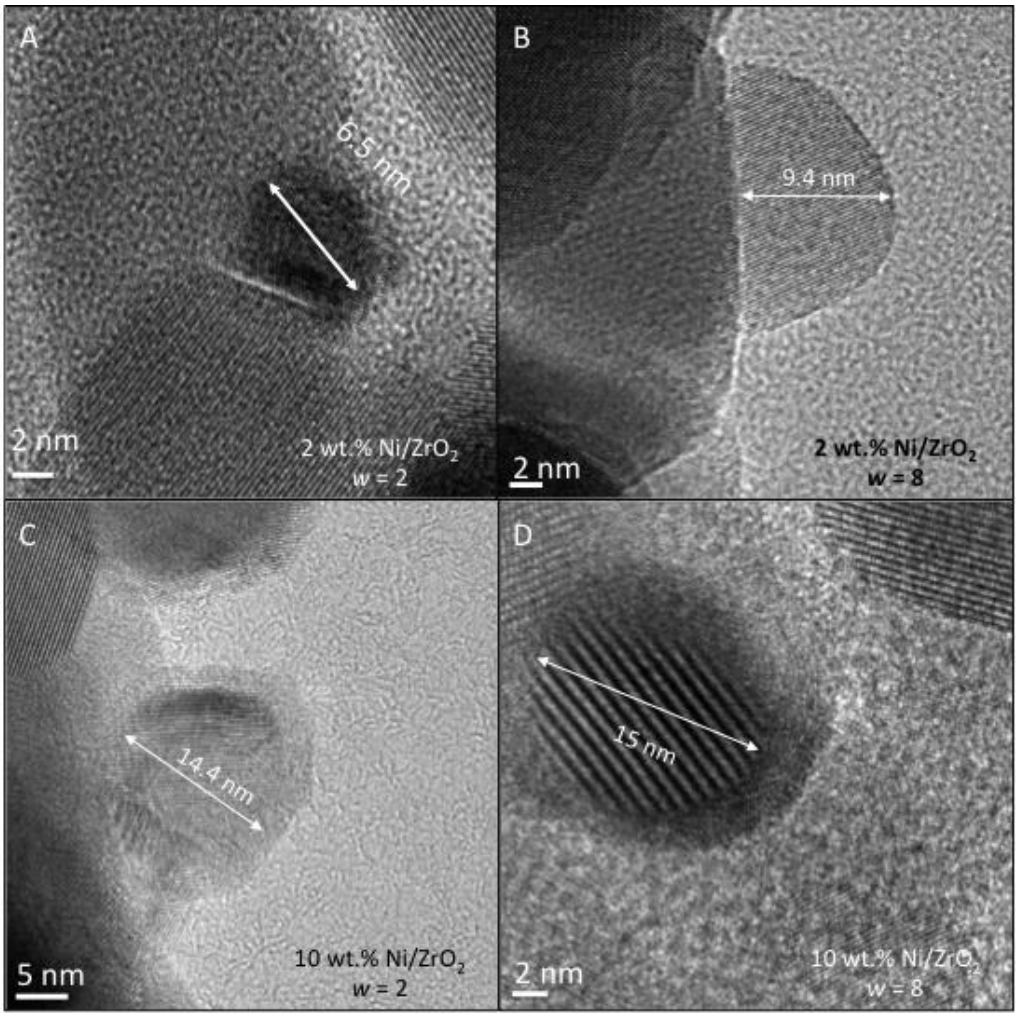


Figure 23. TEM images obtained from MEM samples. The samples were reduced for 30 min at 550 °C in a 50 ml/min pure $H_2$ flow. The figure compares the size of the particles depending on *w* and metal loading in the synthesis. The concentration of surfactant in cyclohexane on the synthesis is 0.5 M. Samples on the right have water content *w* = 2 and samples on the left have *w* = 8. Reduction of the sample prior TEM characterization was performed at 550 °C for 30 min under 50 ml/min flow of pure $H_2$ gas.

The above figure represents the characterization of the samples synthesized with 0.5 M surfactant concentration in cyclohexane. For these series of experiments no Co nanoparticles were found but in this case, in the bimetallic samples TEM images were captured. Part A and part B of Figure 23 compare the size of the particles synthesized with different water content. Section C and D do the same size comparison but 10wt.% samples are used in the synthesis.

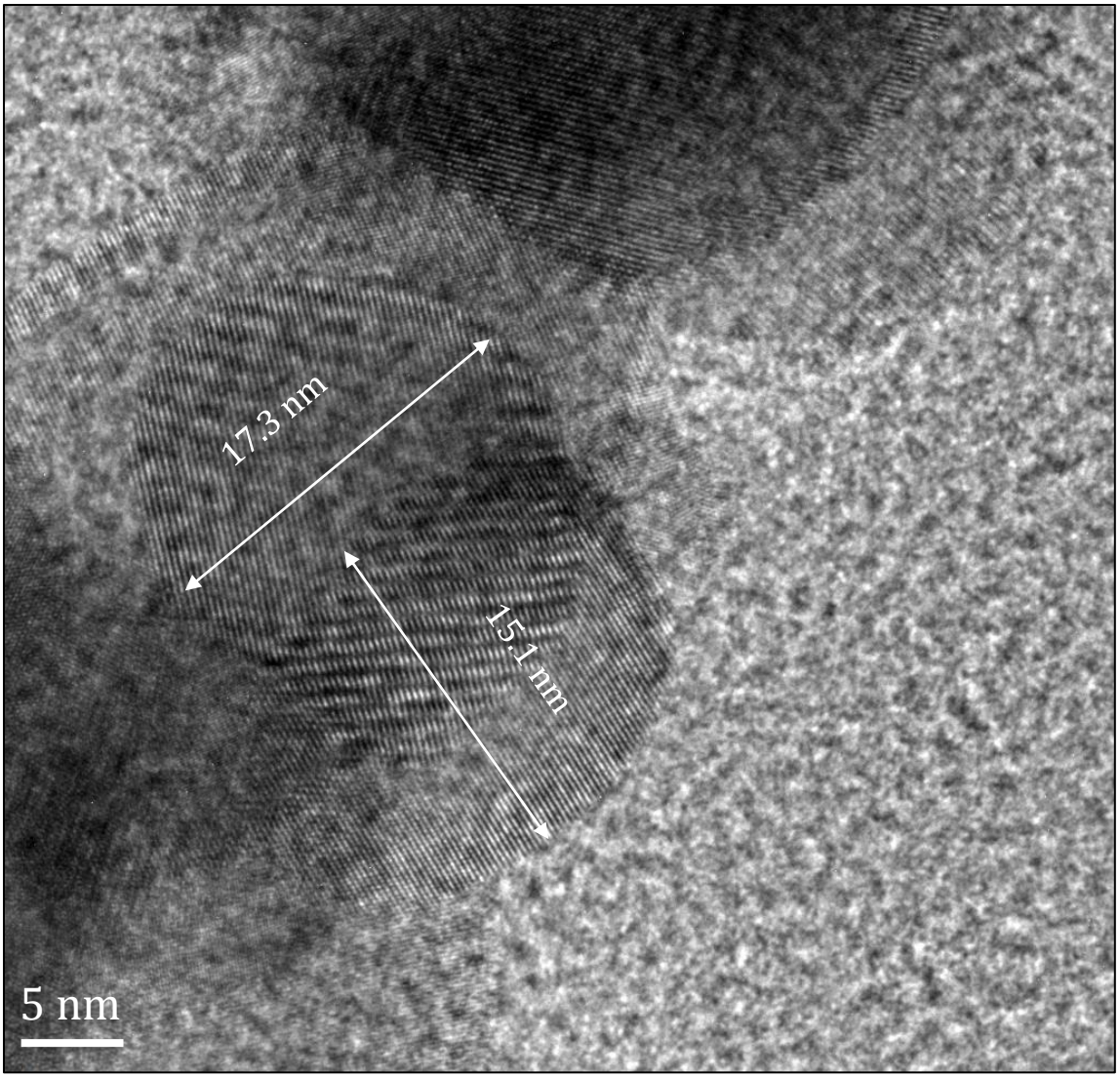


Figure 24. TEM micrograph obtained from a 10 wt.% Co-Ni/$ZrO_2$ sample synthesized using a microemulsion with surfactant concentration in cyclohexane of 0.5 M and $w$ = 8. Reduction of the sample prior TEM characterization was performed at 550 °C for 30 min under 50 ml/min flow of pure $H_2$ gas. Two different nanoparticles are identified in the figure differentiated from the crystallographic pattern observed.

The 10wt.% Co-Ni/ZrO2 sample was characterize with TEM. For the nanoparticles observed in the figure no specific STEM analysis or EDX was performed, therefore is not possible to confirm the alloy of Co-Ni in the nanoparticles observed in Figure 24. The nanoparticles present a similar particle size but a different crystallographic pattern is observed on them.

3.3 One-pot synthesis of supported nickel nanoparticles on silica

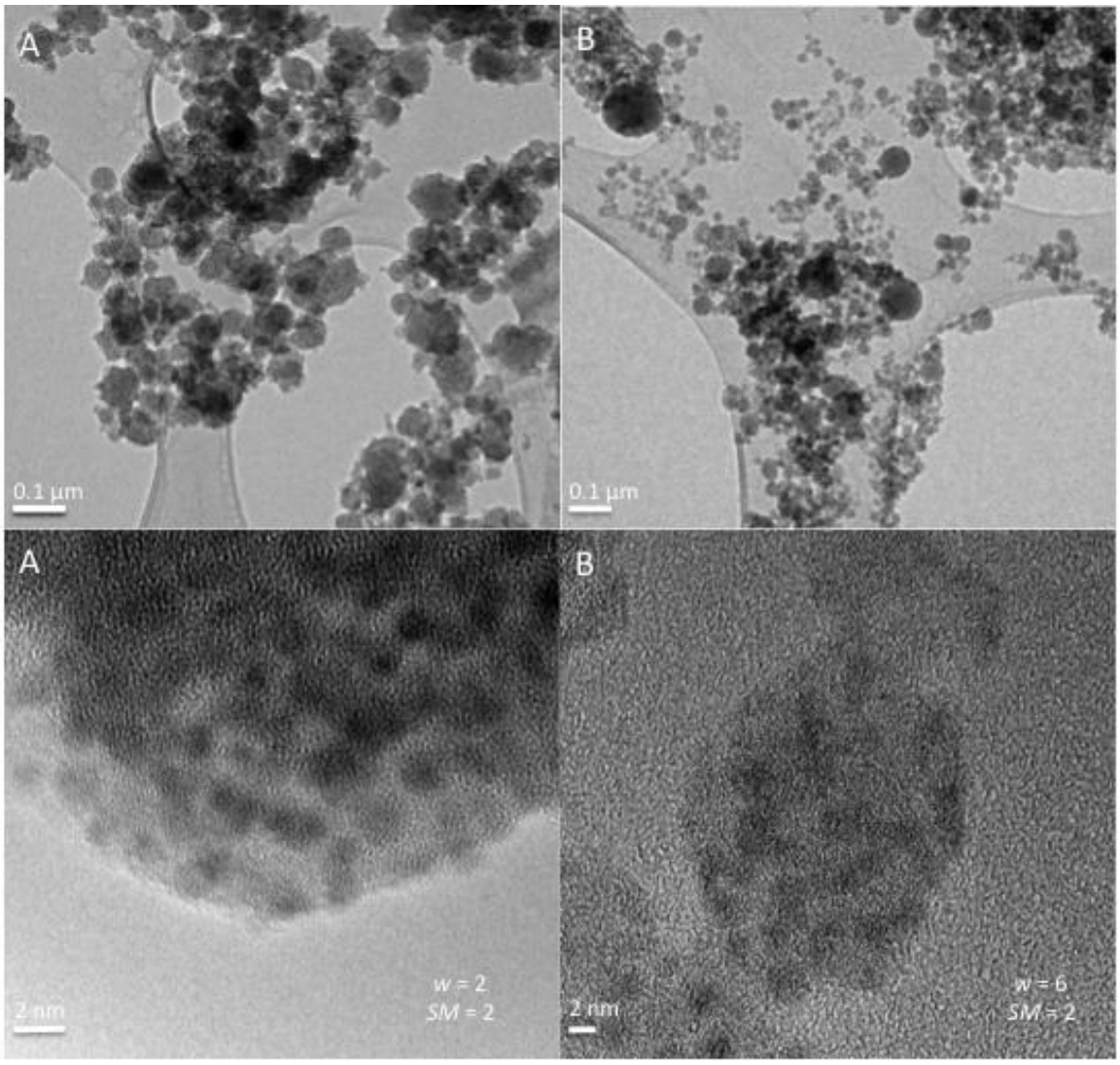


Figure 25. TEM images for two different samples (A and B). The samples are silica particles decorated with nickel nanoparticles. All variables are the same in the synthesis except the water volume in the system.

The TEM analysis of the synthesized samples is shown from Figure 25 to Figure 27. All the samples produced in this series of experiments show nanoparticles of narrow size distribution. The size of the nanoparticles immobilized in the silica spheres is 2 nm; as estimated from the micrographs. The main effect observed due to the difference in water content is the size distribution of the silica

spheres. The size of the silica spheres found for a $w$ = 2 varies approximately from 80 to 100 nm. Relative uniform size distribution is observed for these samples. When the water content is incremented, as shown in sample B of Figure 25, the spheres are polydisperse (35-120 nm). The same sample B is presented in Figure 26 and studied in more detail; the analysis was performed under different beam focus conditions. In a 3 dimensional space, as shown in the insets of the figure the beam was focus on different spots of the sphere. The inset illustrates the spot in which the beam is on focus. The last figure in this section shows the synthesis of large silica spheres. The size is uniform and is estimated to be around 1 μm. A more careful and detailed analysis of the image reveal that this large particles are formed by smaller 20 nm spheres, also uniform in size. Finally, nickel nanoparticles are observed immobilized on the 20 nm silica spheres with a mean particle size of 2 nm.

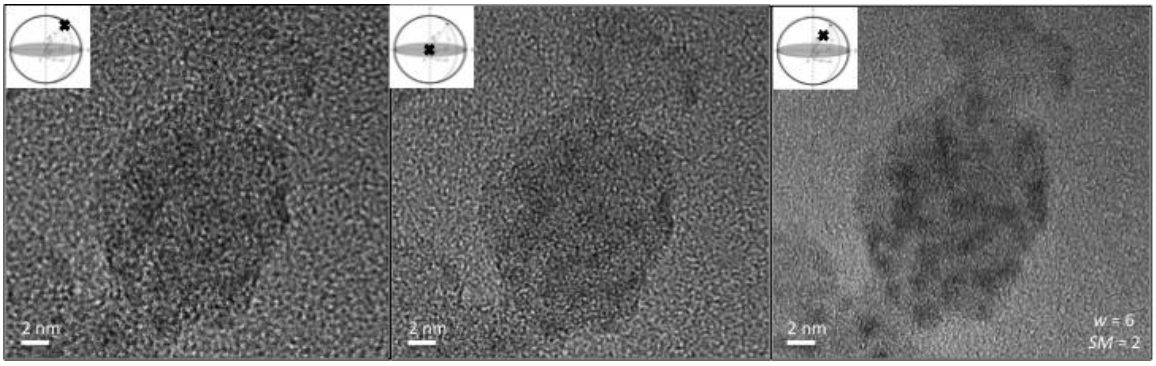


Figure 26. TEM consecutive images of the same observed particle. The beam was focused on different parts of the spherical silica particle. The distance shift is schematically represented in the insets of the figures to illustrate where is the beam focus on the sphere. 2 nm nickel nanoparticles are trapped in the silica matrix.

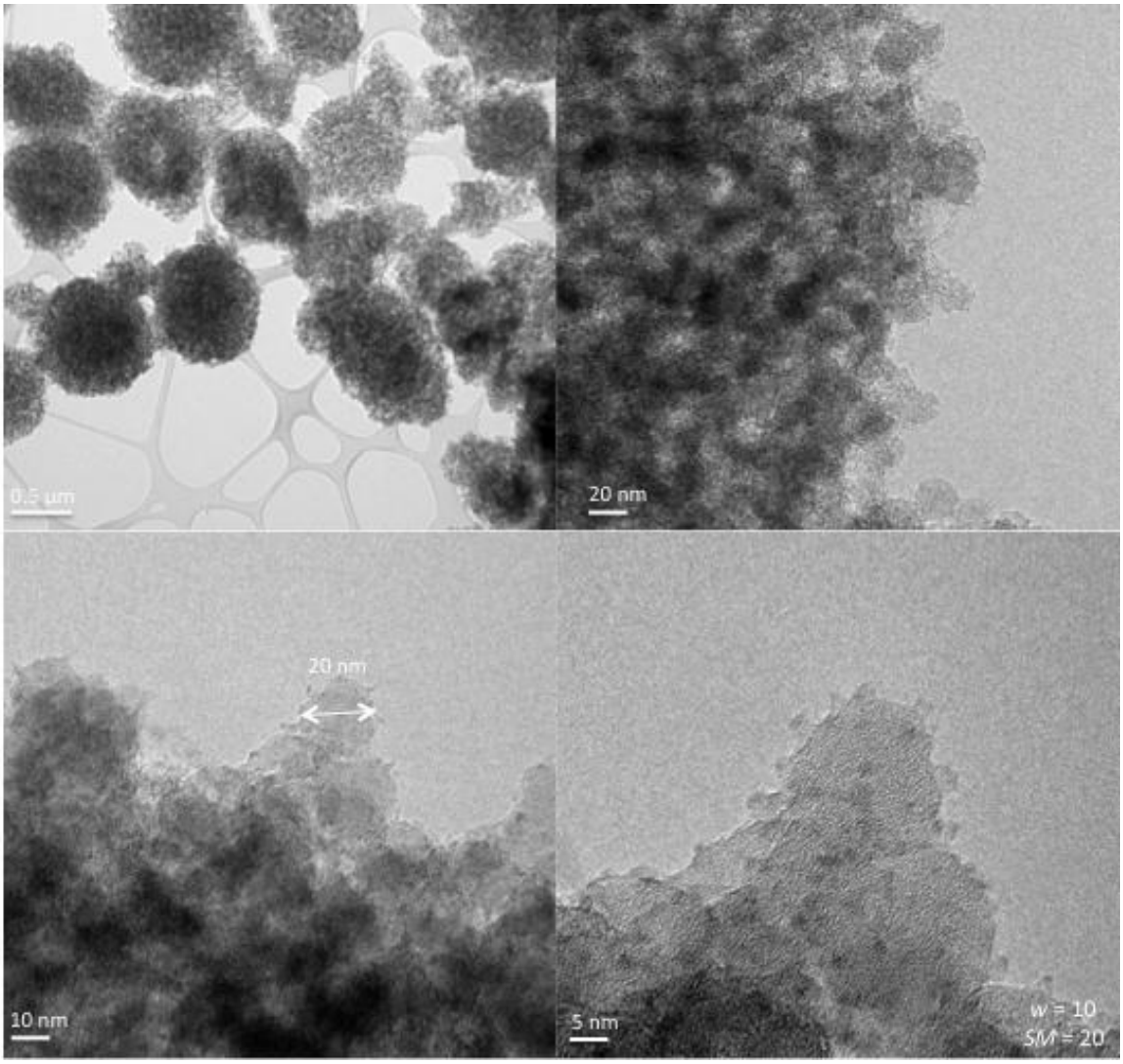


Figure 27. TEM micrograph of the sample aged for 1 week after aqueous ammonia addition. Metal concentration was reduced 10 times in order to obtain *SM* = 20. A Uniform size distribution of 2 nm nickel nanoparticles is observed in the bottom right hand side of the figure. The nanoparticles are homogeneously dispersed on the surface of 20 nm silica spheres.

# 4. Discussion

## 4.1 Size-controlled nickel nanoparticles supported on alumina

The nickel nanoparticles are spherical in morphology and all of the samples show homogeneous size distribution. The nanoparticles found in the

characterization have a size below 10 nm, which it was the desired result of the calculations and the literature review.

In order to achieve the objective of this study, it is necessary to synthesized transition metal nanoparticles with size below 5 nm. The smallest particles observed in this batch are found in the samples with the lowest concentration of nickel as expected. The range of the nanoparticles obtained from this series of experiments range from 4.4 nm to 5.7 nm.

In Figure 12, 2.5 wt.% $Ni/Al_2O_3$ samples were synthesized with different water content in the microemulsion used. The idea is simple, as you input more water in the system, the size of the water "microreactors" will increase. The metal crystal growth is fully constraint by this reactor; thus, if the space is bigger and there is enough concentration of the metal precursor, the particle can grow more.

It is important to mention that the nickel nanoparticles characterized on this study are highly sensitive to the high-energy electron beam of the TEM apparatus. During the observation of the specimen under the microscope it is possible to observe particle aggregation and movement when trying to focus on a specific region of the sample. A clear example is observed in sample A at the right top corner of Figure 12; it is possible to observe a darker region due to the metal aggregation of particles caused by the electron beam. With this in mind, size estimation was performed only on the unperturbed nanoparticles.

Figure 12 shows 4 different samples with different $w$ values ($w_A$, $w_B$, $w_C$ and $w_D$). Sample A shows a particle size of 4.4±0.2 nm but the morphology of the particles is not as clear as in the other micrographs. In sample B aggregated spherical particles

are observe with an approximate particle size of 5.0±0.2 nm. For case C when a bigger particle is expected almost same size particles (5.0±0.3 nm) are observed in the image. Last sample was made with double the amount of metal present in the sample but again, almost same size particles are obtained but the deviation of particle size incremented (5.5±1.7 nm), which means a non-uniform size distribution of the particles present on this sample. From this series of 2.5 wt.% loaded nickel samples the size range obtained goes from 4.4 to 5.7 nanometers.

The analysis of the TEM images gave raise to the possibility of the surfactant still present in the samples. Another question to answer was weather or not the nickel nanoparticles were in the support. The EFTEM/EDX analysis was performed in order to map the elements present in the sample. Nickel and aluminium were observed in the energy dispersion diagram along with oxygen, carbon and cupper. The former two may correspond to the $Al_2O_3$ support, the possible oxidation of the nickel particles or the presence of the surfactant in the sample. Carbon and cupper are expected to appear because of the sample holder.

The main concern with the TEM results is the aggregation of nanoparticles observed in Figure 12. Another important aspect to point out is the size of the synthesized nickel nanoparticles, it can be concluded that there was no significant change in the size of the metal crystals. Moreover, the smallest particles observed in the synthesis are around the 5 nm order. The desired control of particle size would be in the range of 2, 5 and 10 nm.

The amount of nickel present in the synthesis was reduced for the next series of experiments. The loading of the samples presented in Figure 14 was 0.5 wt.%

$Ni/Al_2O_3$. The water content was selected to be $w$ = 4, 8, 16 and 20. The images show that no significant change in the size of the nanoparticles was achieved, even in the highest content of water in section D. The result can be explained with the assumption that there is not enough metal content to grow the particles. Even under this low metal concentration conditions the smallest particle obtained was 4 nm. Furthermore, aggregation of the nanoparticles can result in the lost of size control reflected in the result of obtaining the same particle size.

## 4.2 Nickel, cobalt, iron and cobalt-nickel nanoparticles supported on zirconia

Aggregation of the nanoparticles was previously observed for the alumina support case, while following the most common method found in the literature for supporting the MEM nanoparticles. This method proposes to support the nanoparticles by adding the support directly to the MEM system and then destabilizing it with the addition of a polar solvent like ethanol, acetone or THF.

It was already shown in chapter IV that the MEM system is able to control and restrict the size of the formed nanoparticles inside the reverse micelles. The synthesis method presented here was developed in order to keep the size of the nanoparticles obtained by the standard microemulsion method and to avoid aggregation.

The strategy followed was to carefully control the disequilibrium of the MEM system and to promote the rapid adsorption of the nanoparticles into the oxide support. The hypothesis is that under the described conditions in the experimental procedure section; one drop of the microemulsion system, containing the stabilized

nanoparticles, will encounter a huge volume of polar solvent and will quickly destabilize the formed micelles generating the liberation of the nanoparticles in the solution containing the dispersed support. Then, by precisely controlling the concentration gradient in the support solution, is possible to carefully destabilize the MEM system to our advantage.

The first experiment performed was TGA to determine the best calcination temperature in order to finish the synthesis process of the samples. The objective was also to investigate the carbon content of the samples after filtration and washing. TGA results showed the presence of 1 to 8 wt.% of carbon present with respect of the total weight of the sample. It can be discussed from Figure 15 that all samples show the complete removal of carbon above a 400°C temperature. Therefore, the calcination step in the synthesis process for supported transition metal nanoparticles was selected to be performed at 450 °C for 3 h in order to assure the complete removal of the remaining carbon compounds in the samples.

The metal content and the synthesis conditions were the same for all the samples exposed on Figure 15. From the TGA figure, it is noticeable the big difference in carbon content found between, for example, Co and Fe or Ni and Co-Ni. After repeated steps of washing with ethanol as a solvent for removing the remaining surfactant; a huge amount of carbon is still present in the 2 wt.% $Co/ZrO_2$ sample (8% of the total weight). With a similar result, the 2 wt.% $Ni/ZrO_2$ sample was found to have 6% of carbon weight. The results indicate that the washing procedure was not enough for removing the surfactant, thus a temperature treatment was required.

In order to determine the actual metal weight percentage of the samples two experiments were performed. First, SEM apparatus coupled with an EDX system were utilized to identify the elemental composition of the samples. Later, TPR experiments were used to estimate the metal content of the samples.

EDX energy distributions were recorded using the SEM apparatus. The software of the detection system permits the fitting of a curve in the energy peaks distribution in order to, not only qualitatively analyze which element is present in the samples, but also to perform a quantification of the intensity of the peaks and estimate the weight percentage of each element present in the sample. The results are shown in Appendix F and the estimation shows agreement with the theoretical metal content during the synthesis. The 2 wt.% Ni, Co and Co-Ni samples show the same weight percentage of the element present in the EDS energy distribution. The nickel sample estimation was in 2 wt.% exactly, while the Co sample overestimates the content in 2.1 wt.% and finally the Co-Ni sample estimation was not as successful indicating a 2.4 wt.% of cobalt with only 0.4 wt.% of Ni present in the sample. EDX analysis is shown in Appendix F.

Using the TPR profiles obtained in Figure 20 and using a known reference sample the metal content was determined. The calculations were done comparing the Hydrogen uptake of the metals assuming a complete reduction of the particles and 1:1 metal to hydrogen stoichiometry ratio as shown for example in E 6.

$$NiO + H_2 \rightarrow Ni + H_2O \qquad \text{E 6}$$

A known amount of commercial NiO was mixed with zirconia and under the same experimental conditions the TPR profiles were recorded. From this known sample reference, calculations were performed and their TPR profiles are presented in Appendix E. By using the area of the curves it was possible to compare and quantify the metal content of the samples prepared with the microemulsion synthesis. The TPR profile of the MEM samples was correlated and the metal content in weight percentage was estimated. The results show good agreement with the designed values of the synthesis. The nickel and the cobalt-nickel sample present a 1.6 wt.% of metals in the support while the cobalt monometallic samples was estimated in 1.9 wt.%. These calculations are only estimations and do not represent an accurate calculation of the metal content of the catalysts, but it represents a simple and efficient method for proving the presence of the metals supported and the interaction of the particles with the support.

The TPR profiles analyzed in Figure 20 show first, the interaction of the metal nanoparticles with the support. The physically mixed sample of NiO starts reducing little after 300°C and the reduction peak appears to finish just below 450°C. In contrast, the 2 wt.% Ni loaded sample obtained with the MEM method shows a delay of a little more of 50°C in the reduction peak. This is an indication of the interaction of the metal nanoparticles with the support. The next pattern from top to bottom Figure 20 represents the reduction of the cobalt sample. The diagram shows two reduction peaks, the first one with maxima at 400°C and the second one with maxima above 600°C. These two peaks are attributed to first the reduction of

$Co_3O_4$ species to CoO; then, the reduction of CoO to $Co^{(0)}$ is achieve and represented by the second reduction peak. The cobalt sample is the one showing higher reduction temperature with the second reduction peak starting late at 500°C and ending around 700°C. The last profile at the bottom of the figures shows the beneficial result of the cobalt and nickel interaction in the sample. The profile illustrates three reduction peaks, which are in this work assigned correspondently to the reduction of NiO to $Ni^{(0)}$ and the consequent reduction of $Co_3O_4$ – CoO – $Co^{(0)}$. The first reduction peak starts earlier than the physically mixed sample around 250°C and finish below the 350°C. The second peak maxima is found at 400 °C and the third peak maxima just above 500 °C. In comparison with the Co sample, the third peak maximum was significantly reduced. The meaning of the result found in the bimetallic sample indicates that the Co-Ni interaction improves the reducibility of the catalyst significantly.

Before discussing the TEM results, it is necessary to point out that the preparation of the TEM samples needs to be further optimized to avoid possible particle agglomeration. Furthermore, a sample holder with a controlled atmosphere could have been beneficial for the goals of this research. As mentioned earlier in this work, the oxidation of the metal nanoparticles is expected due to the synthesis and sample preparation conditions.

The TEM results showed in Figure 22 represents the synthesized samples under the 0.87 M surfactant concentration, which have been already characterized previously with different experimental techniques. TEM images of the cobalt and cobalt-nickel samples with a 2 wt.% loading and $w$ = 4 were not successfully

characterize with TEM because the nanoparticles were challenging to be idenfied. The figure shows the nanoparticles found in 2 wt.% $Ni/ZrO_2$ and 2 wt.% $Fe/ZrO_2$ samples both with $w$ = 4. The result obtained from the iron sample was very interesting because the size of the particles found was around 2 nm. In contrast most particles observed for the nickel samples have a mean of 5 nm. From the results is possible to think in a second step aggregation process, which doesn't appear to affect the iron nanoparticles. In order to further discuss more in this subject the next TEM characterization of the second batch of experiments was performed.

Figure 23 and Figure 24 illustrate the samples synthesized with a 0.5 M surfactant concentration in the microemulsion. The results show the importance of the surfactant not only as a cage for containing the water droplets in which the nanoparticles are grown; but also it is possible that the surfactant plays a ligand-like stabilizing role for further aggregation steps that may occur in the synthesis. Section A of Figure 23 shows that under same synthesis conditions, except for the surfactant concentration, the size of the observed particles in a 2 wt.% sample with even less water content than before (i.e. $w$ = 2) bigger particles are obtained with approximately 6 nm in size. This arise the conclusion that if the surfactant presence is high enough smaller particles will be obtained. In the literature, ligands are used to stabilize the particles in the suspension. In this experiment, the surfactant could play the role of a direct stabilizer of the metal particles. Micelles in the microemulsion are in constant and dynamic collision; once the metal nanoparticle nucleation is achieved the growth happens due to the collision and diffusion of the

reactants in the water pool. The generally accepted role of the surfactant is to create a constrained space for the particle to grow until a specific size is achieved, not directly related with the water pool size. In the method developed on this research a subsequent step is performed in order to support the nanoparticles. It is assumed that the nanoparticles will not aggregate during this step, but apparently they do. Moreover, here the surfactant concentration may play a second role of limiting the growth of the particles like observed from the size difference of the micrographs in Figure 22.A and Figure 23.A.

Analyzing more of Figure 23, the section B shows the size of the nickel nanoparticle found is around 9 nm. Following this comparison, part C and D also compares the size control of 10 wt.% Ni samples. When saturating the MEM system only a small range of control is achieved, the same happens when having a very low metal concentration of the precursors as previously observed with the alumina supported sample in Figure 12 and Figure 14. Therefore, it may possible to obtain smaller particles but size control range would be limited.

### 4.3 One-pot synthesis of supported nickel nanoparticles on silica

The first important point to discuss in the experiments is the observation that the water content did not cause any effect in the particle size control. When changing the water volume in the synthesis the same size of nickel nanoparticles was found in all the micrographs. This can be attributed to another element affecting the control of the particle size: the reduction reagent.

The reduction agent concentration can play a decisive role in the particle size control. The $NaBH_4$/Metal molar ratio parameter determines the kinetics of nucleation of the metal particles; thus, if the nucleation is extremely fast the size of the metal nanoparticle cannot grow further. This hypothesis was formulated from similar results found in the literature when using a high reducing agent-to-metal molar ratio.

The effect of water is critical for the final size of the silica particles. For the objectives of this research, the size of the support particles is not critical. However, is important to mention that the water content is an important parameter for controlling the hydrolysis of the alkoxide silica precursor. A very interesting result was the effect of time in the synthesis. For the first samples, 18 h were enough to trap the nanoparticles in the silica sphere; with some nanoparticles exposed in the surface. In contrast, after 1 week the silica spheres grow to a final size of 20 nm with the nickel nanoparticles homogeneously distributed in the surface of the support. Apparently the silica spheres self-organize themselves into bigger silica particles with a mean diameter of 1 μm.

## 5. Conclusion

### 5.1 Size-controlled nickel nanoparticles supported on alumina

Nickel nanoparticles on alumina are found to have a uniform size distribution with an average size of 5 nm. The effect of different variables in the synthesis was studied and the reaction conditions can be optimized in order to obtain smaller

crystals. Metal concentration in the sample is important in order to obtain a good dispersion of active metal centers. The size of the surfactant molecule and its concentration plays an important role in determining the size of the metal particles as compared when using NP5 or BRIJ-30. The synthesis process needs further optimization in order to avoid particle agglomeration. The aggregation phenomena may occur during the destabilization step when attempting to support the nanoparticles into alumina. For the following section the reaction condition will be improved in order to obtain a wider size control range, smaller nanoparticles and finally the establishment of a modified and novel microemulsion general method for obtaining supported and size-controlled transition metal nanoparticles.

## 5.2 Nickel, cobalt, iron and cobalt-nickel nanoparticles supported on zirconia

Different size nanoparticles were supported on zirconia. TGA experiments calculations demonstrated the carbon content of the samples and determined the calcination temperature for the last part of the synthesis process. A more detailed characterization was performed on the microemulsion-produced catalysts. XRD identified the oxidation state of the metals due to the synthesis conditions. TPR profiles helped with the calculation of the actual metal weight percentage found in the samples. The TPR experiments showed clearly the synergetic effect of the cobalt-nickel interaction in the bimetallic sample, which improves significantly the reducibility of the catalyst. HRTEM images identified the size of the obtained supported nanoparticles in the samples. The role of the metal precursor concentration and the surfactant concentration in the synthesis was discussed in

more detail on this chapter. Further improvements and more investigations are needed to clearly define how the aggregation of the particles is taking place and to prove the ligand-like role of the surfactant in the support step. Finally, samples with size-controlled nanoparticles supported in zirconia were successfully synthesized by a modified microemulsion method, obtaining a narrow size distribution and a control range of 5 nm to 17 nm.

## 5.3 One-pot synthesis of supported nickel nanoparticles on silica

In the microemulsion each nanoparticle is isolated by the surfactant, this cage-like situation is desirable for controlling the dispersion of the nanoparticles in the surface of the support. Thus, it was proposed that the support was synthesized inside the microemulsion system. First, the proper alkoxide precursor of the support must be selected. In this case, TEOS was selected in order to obtain nickel nanoparticles supported in $SiO_2$. The alkoxide is then dissolved in the oil phase of the microemulsion; later, the alkoxide will undergo hydrolysis with the water phase present in the system. The support particle will grow under the presence of the organize microemulsion system and the nanoparticles are expected to absorb in the surface. Finally the product is precipitated and washed several times. Figure 27 is the prof-of-concept of the hypothesis developed during the ongoing part of the study. The figure shows uniformly disperse nickel nanoparticle with a homogeneous size distribution of 2 nm decorating 20 nm silica spheres. The 20 nm silica spheres later undergo a self-assembly step producing big silica spheres of 1 μm. This method

represents a practical strategy to study particle size effects of different metals supported on oxidic supports.

The novel method presented here was developed but not optimized due to time constraints. A low yield of product can be obtained from the synthesis method. Further characterization and application of the samples is needed in order to optimize the synthesis technique developed on this section. Likewise, more improvements are required in order to study the size effect related with the reducing agent concentration. A more detailed study is needed in the grow mechanism of silica particles. evolution of silica particles.

## VI. Summary

In the field of heterogeneous, design of the active sites in controlled size and morphology is more and more desired. Size control of metal particles is one of the most common and important tasks to be achieved. It is a big challenge to precisely control the size of immobilized non-noble nanoparticles under a 10 nm range. The microemulsion system with reverse micelles structure was used to control the size of non-noble metal nanoparticles. Furthermore, a new synthesis technique was developed to achieve immobilization and size-control at the same time.

The microemulsion system formed with cyclohexane, BRIJ-30 surfactant and water was described in chapter 3. The studied parameters were the water content ($w$) and metal precursor concentration. The water content is directly related with the control of the particle size; as the water volume inside the reverse micelle increased, the size of the final nanoparticles increased as well. The results obtained showed a size control between 5 and 35 nm when the water content was varied from $w = 2$ to $w = 10$. The metal concentration in the microemulsion also plays an important role to control the size. If there is sufficient space for the particle size to grow ($w$), but not enough metal precursors the final particles will not reached the designed size.

Chapter 4 presents the immobilization methods for supporting size-controlled non-noble metal nanoparticles on oxidic supports. The immobilization techniques are based on the microemulsion method and take advantage of the self-

organized nature of the system. In the first part of the chapter, nickel nanoparticles supported on aluminium oxide were synthesized using a microemulsion formed with NP5 surfactant. The first method consisted in adding the support directly to the microemulsion containing the reduced nanoparticles, followed by the precipitation of the nanoparticles on the support and finally, the recovery of the product. The size of the particles observed with TEM has a narrow size distribution. However, no clear particle size control was achieved. In a regular synthesis, the size control obtained was in the range of 4.7-5.7 nm. Moreover, aggregation of the nanoparticles was observed in the samples. The aggregation occurs during the immobilization step of the synthesis. For catalytic application purposes, supported nanoparticles in this state are not desirable.

The second method was designed to solve the aggregation problem. In this procedure, the microemulsion is drop-by-drop added to an ethanol solution of the support. In this way concentration gradients are avoid and a careful control of the adsorption of the nanoparticles on the support is achieve. Nickel, cobalt, iron and cobalt-nickel nanoparticles were supported on zirconia with a precise size control. The effect of surfactant concentration was clarified with TEM size characterization. Low surfactant concentration (0.5 M) lead to a size control between 6 and 17 nm, while high surfactant concentration (0.87 M) produced smaller Ni nanoparticles of 5 nm. The final size of the particle also depends on the nature of the metal. Supported 2 nm Fe nanoparticles were obtained under the same reaction conditions as the 5 nm Ni samples. Characterization of the catalyst obtained was performed. TGA results showed a considerable amount of carbon (≤8 wt.%) present in the samples.

It was not possible to remove the surfactant by washing and a calcination step above 400°C was required. TPR was used to calculate the loading yield of the immobilization method and it was found that 85% to 95% of the amount of metal used for synthesis is obtained in the final product. TPR showed that the reducibility of the catalyst was improved with Co-Ni supported nanoparticles. Ni nanoparticles start to reduce at 350°C while in the Co-Ni case the reduction starts at 250°C. XRD identified NiO and $Co_3O_4$ oxide phases of the nanoparticles.

The final method is a novel one-pot synthesis of nanoparticles and the support. In this method, an alkoxide support precursor is added in the microemulsion system. The precursor hydrolyzes in the presence of the homogeneously distributed metal particles producing the immobilization of the nanoparticles in the same synthesis reaction. Synthesis conditions were designed with high BRIJ-30 concentration and a TEOS to Ni molar ratio of 20. Figure 27 illustrates the proof-of-concept of the method. This novel methodology was used to produced uniformly disperse Ni nanoparticles with homogeneous size distribution of 2 nm covering the surface of 20 nm silica spheres.

In conclusion, size controlled Ni, Co, Fe and Co-Ni nanoparticles were supported on alumina, zirconia and silica supports using the microemulsion system. The nanoparticles have a narrow size distribution and are uniformly disperse on the supports. A new methodology for producing size-controlled supported metal nanoparticles was nearly established. The novel method is applicable to the synthesis of size-controlled nanoparticles irrespectively from the support or the nature of the metal utilized. Therefore, it is a flexible and robust methodology,

offering the possibility of studying the nanoparticles size effects present in different catalytic reactions and metal-support interactions.

The control of the particle size achieved with the methods presented on this study is in the range of 2 to 17 nm. The characterization of the nanometer-sized non-noble metal supported catalysts showed promising thermal and chemical properties for catalytic applications. Although the product yield is low, further optimizations can be done. To the best of my knowledge there is no report in the synthesis of both support and metal active centers in the same synthesis reaction.

A deeper understanding of the microemulsion itself is still required and further investigations can be done to reveal the role of the reducing reagent in the final size of the particles, the possible function of the surfactant as a ligand in the surface of the metals and, finally the role of the organic solvent in the final size and morphology of the support.

## REFERENCES


1. Rothenberg, G. *Catalysis. Concepts and Green applications*. 231(2008).

2. Armor, J.N. Environmental catalysis. *Applied Catalysis B: Environmental* **1**, 221-256(1992).

3. Centi, G. et al. Environmental catalysis: trends and outlook. *Catalysis Today* **75**, 3-15(2002).

4. Zhou, B. et al. *Nanotechnology in Catalysis*. 322(Springer: 2007).

5. Shi, F. et al. Tuning catalytic activity between homogeneous and heterogeneous catalysis: improved activity and selectivity of free nano-Fe2O3 in selective oxidations. *Angewandte Chemie (International ed. in English)* **46**, 8866-8(2007).

6. Wang, C. et al. A General Approach to the Size- and Shape-Controlled Synthesis of Platinum Nanoparticles and Their Catalytic Reduction of Oxygen. *Angewandte Chemie* **120**, 3644-3647(2008).

7. Johnson, B.F.G. Nanoparticles in Catalysis. *Topics in Catalysis* **24**, 147-159(2003).

8. Grenoble, D. The chemistry and catalysis of the toluene hydrodealkylation reaction I. The specific activities and selectivities of Group VIIB and Group VIII metals supported on alumina. *Journal of Catalysis* **56**, 32-39(1979).

9. Ishihara, T., Eguchi, K. & Arai, H. Hydrogenation of Carbon Monoxide SiO2-Supported Fe-Co, Co-Ni and Ni-Fe bimetallic Catalyst. *Applied Catalysis* **30**, 225-238(1987).

10. Wrobleski, J.T. & Boudart, M. Preparation of Solid Catalysts: An appraisal. *Catalysis today* **15**, 349–360(1992).

11. Nagaoka, K. Modification of Co/TiO2 for dry reforming of methane at 2MPa by Pt, Ru or Ni. *Applied Catalysis A: General* **268**, 151-158(2004).

12. Takanabe, K. & Iglesia, E. Rate and selectivity enhancements mediated by OH radicals in the oxidative coupling of methane catalyzed by Mn/Na2WO4/SiO2. *Angewandte Chemie (International ed. in English)* **47**, 7689-93(2008).

13. Huang, Y. & Schwarz, J. The effect of catalyst preparation on catalytic activity: I. The catalytic activity of Ni/Al2O3 catalysts prepared by wet impregnation. *Applied catalysis* **30**, 239–253(1987).

14. Huang, Y.J.R., Barrett, B. & Schwarz, J. The effect of solution variables on metal weight loading during catalyst preparation. *Applied catalysis* **24**, 241–248(1986).

15. Pinna, F. Supported metal catalysts preparation. *Catalysis Today* **41**, 129-137(1998).

16. Xue, M. et al. Preparation of highly loaded and dispersed Ni/SiO2 catalysts. *Catalysis Communications* **12**, 332-336(2011).

17. Fang, B. et al. Homogeneous deposition of platinum nanoparticles on carbon black for proton exchange membrane fuel cell. *Journal of the American Chemical Society* **131**, 15330-8(2009).

18. Bezemer, G. et al. Preparation of Fischer–Tropsch cobalt catalysts supported on carbon nanofibers and silica using homogeneous deposition-precipitation. *Journal of Catalysis* **237**, 291-302(2006).

19. Bitter, J. et al. Synthesis of highly loaded highly dispersed nickel on carbon nanofibers by homogeneous deposition–precipitation. *Catalysis letters* **89**, 139–142(2003).

20. Park, K.H., Im, S.H. & Park, O.O. The size control of silver nanocrystals with different polyols and its application to low-reflection coating materials. *Nanotechnology* **22**, 045602(2011).

21. Yan, X., Liu, H. & Liew, K.Y. Size control of polymer-stabilized ruthenium nanoparticles by polyol reduction. *Journal of Materials Chemistry* **11**, 3387–3391(2001).

22. Joseyphus, R.J. et al. Size controlled Fe nanoparticles through polyol process and their magnetic properties. *Materials Chemistry and Physics* **123**, 487-493(2010).

23. Srivastava, M., Chaubey, S. & Ojha, A.K. Investigation on size dependent structural and magnetic behavior of nickel ferrite nanoparticles prepared by sol–gel and hydrothermal methods. *Materials Chemistry and Physics* **118**, 174-180(2009).

24. Du, H. et al. A facile synthesis of highly water-soluble, core-shell organo-silica nanoparticles with controllable size via sol-gel process. *Journal of colloid and interface science* **340**, 202-8(2009).

25. Zhang, Y. et al. Synthesis of monodisperse Ce x Zr1−x O2 nanocrystals and the size-dependent enhancement of their properties. *Nano Research* **4**, 494-504(2011).

26. Zhang, Q., Xie, J. & Yang, J. Monodisperse icosahedral Ag, Au, and Pd nanoparticles: size control strategy and superlattice formation. *ACS nano* **3**, 139-148(2008).

27. Horikoshi, S. et al. Access to small size distributions of nanoparticles by microwave-assisted synthesis. Formation of Ag nanoparticles in aqueous carboxymethylcellulose solutions in batch and continuous-flow reactors. *Nanoscale* **2**, 1441-7(2010).

28. Kundu, P. et al. Ultrafast Microwave-Assisted Route to Surfactant-Free Ultrafine Pt Nanoparticles on Graphene : Synergistic Co-reduction Mechanism and High Catalytic Activity. *Chemistry of Materials* **23**, 2772-2780(2011).

29. Gardner, J.S. et al. Rapid synthesis and size control of CuInS2 semi-conductor nanoparticles using microwave irradiation. *Journal of Nanoparticle Research* **10**, 633-641(2007).

30. Peng, Z. & Yang, H. Designer platinum nanoparticles: Control of shape, composition in alloy, nanostructure and electrocatalytic property. *Nano Today* **4**, 143-164(2009).

31. Kahn, M.L. et al. Organometallic chemistry: an alternative approach towards metal oxide nanoparticles. *Journal of Materials Chemistry* **19**, 4044(2009).

32. Satoh, N. et al. Quantum size effect in TiO2 nanoparticles prepared by finely controlled metal assembly on dendrimer templates. *Nature nanotechnology* **3**, 106-11(2008).

33. Rubio-Garcia, J. et al. One-step synthesis of metallic and metal oxide nanoparticles using amino-PEG oligomers as multi-purpose ligands: size and shape control, and quasi-universal solvent dispersibility. *Chemical communications (Cambridge, England)* **47**, 988-90(2011).

34. Shulman, J.H. & Hoar, T.P. Transparent water-in-oil dispersions: the oleophatic hydro-micelle. *Nature* **152**, 102-103(1943).

35. Ganguli, A.K., Ganguly, A. & Vaidya, S. Microemulsion-based synthesis of nanocrystalline materials. *Chemical Society reviews* **39**, 474-85(2010).

36. Eriksson, S. Preparation of catalysts from microemulsions and their applications in heterogeneous catalysis. *Applied Catalysis A: General* **265**, 207-219(2004).

37. Boutonnet, M., Lögdberg, S. & Elm Svensson, E. Recent developments in the application of nanoparticles prepared from w/o microemulsions in heterogeneous catalysis. *Current Opinion in Colloid & Interface Science* **13**, 270-286(2008).

38. Uskoković, V. & Drofenik, M. Reverse micelles: inert nano-reactors or physico-chemically active guides of the capped reactions. *Advances in colloid and interface science* **133**, 23-34(2007).

39. Zhao, C.-X. et al. Nanoparticle synthesis in microreactors. *Chemical Engineering Science* **66**, 1463-1479(2011).

40. Yadav, O. Synthesis of platinum nanoparticles in microemulsions and their catalytic activity for the oxidation of carbon monoxide. *Colloids and Surfaces A: Physicochemical and Engineering Aspects* **221**, 131-134(2003).

41. Zhang, W., Qiao, X. & Chen, J. Synthesis of silver nanoparticles—Effects of concerned parameters in water/oil microemulsion. *Materials Science and Engineering: B* **142**, 1-15(2007).

42. Yoon, B. & Wai, C.M. Microemulsion-templated synthesis of carbon nanotube-supported pd and rh nanoparticles for catalytic applications. *Journal of the American Chemical Society* **127**, 17174-5(2005).

43. Chen, D.-H. & Wu, S.-H. Synthesis of Nickel Nanoparticles in Water-in-Oil Microemulsions. *Chemistry of Materials* **12**, 1354-1360(2000).

44. Zhang, X. & Chan, K.-Y. Water-in-Oil Microemulsion Synthesis of Platinum−Ruthenium Nanoparticles, Their Characterization and Electrocatalytic Properties. *Chemistry of Materials* **15**, 451-459(2003).

45. Scano, A. et al. Mn–ferrite nanoparticles via reverse microemulsions: synthesis and characterization. *Journal of Nanoparticle Research* **13**, 3063-3073(2011).

46. Smetana, A.B. et al. Fine-tuning size of gold nanoparticles by cooling during reverse micelle synthesis. *Langmuir : the ACS journal of surfaces and colloids* **23**, 10429-32(2007).

47. Dodoo-Arhin, D. et al. Synthesis, characterisation and stability of Cu2O nanoparticles produced via reverse micelles microemulsion. *Materials Chemistry and Physics* **122**, 602-608(2010).

48. Han, D. et al. Controlled synthesis of CuO nanoparticles using TritonX-100-based water-in-oil reverse micelles. *Powder Technology* **185**, 286-290(2008).

49. Osseo-Asare, K. & Arriagada, F.J. Preparation of SiO2 nanoparticles in a non-ionic reverse micellar system. *Colloids and Surfaces* **50**, 321-339(1990).

50. Huang, N.M. et al. Single w/o microemulsion templating of CdS nanoparticles. *Journal of Materials Science* **39**, 2411-2415(2004).

51. Caponetti, E. et al. Microwave-assisted synthesis of anhydrous CdS nanoparticles in a water-oil microemulsion. *Journal of colloid and interface science* **304**, 413-8(2006).

52. Emin, S.M. et al. Growth kinetics of CdSe nanoparticles synthesized in reverse micelles using bis(trimethylsilyl) selenium precursor. *Central European Journal of Chemistry* **5**, 590-604(2007).

53. Solanki, J.N., Sengupta, R. & Murthy, Z.V.P. Synthesis of copper sulphide and copper nanoparticles with microemulsion method. *Solid State Sciences* **12**, 1560-1566(2010).

54. Solla-Gullón, J. et al. Synthesis and structural, magnetic and electrochemical characterization of PtCo nanoparticles prepared by water-in-oil microemulsion. *Journal of Nanoparticle Research* **12**, 1149-1159(2009).

55. Nagy, J.B. Multinuclear NMR characterization of microemulsions: Preparation of monodisperse colloidal metal boride particles. *Colloids and Surfaces* **35**, 201-220(1989).

56. Pramanik, S. & Bhattacharya, S.C. Size tunable synthesis and characterization of cerium tungstate nanoparticles via H2O/AOT/heptane microemulsion. *Materials Chemistry and Physics* **121**, 125-130(2010).

57. Cheney, B. a, Lauterbach, J. a & Chen, J.G. Reverse micelle synthesis and characterization of supported Pt/Ni bimetallic catalysts on γ-Al2O3. *Applied Catalysis A: General* **394**, 41-47(2011).

58. Cheney, B.A., Lauterbach, J.A. & Chen, J.G. Reverse micelle synthesis and characterization of supported Pt/Ni bimetallic catalyst on gamma-Al2O3. *Applied Catalysis A: General* **394**, 41-47(2010).

59. Vestal, C.R. & Zhang, Z.J. Synthesis of CoCrFeO 4 Nanoparticles Using Microemulsion Methods and Size-Dependent Studies of Their Magnetic Properties. *Chemistry of Materials* **14**, 3817-3822(2002).

60. Agnoli, F., Zhou, W.L. & O'Connor, C.J. Synthesis of Cubic Antiferromagnetic KMnF3 Nanoparticles Using Reverse Micelles and Their Self-Assembly. *Advanced Materials* **13**, 1697-1699(2001).

61. Xu, P., Han, X. & Wang, M. Synthesis and Magnetic Properties of BaFe12O19 Hexaferrite Nanoparticles by a Reverse Microemulsion Technique. *Journal of Physical Chemistry C* **111**, 5866-5870(2007).

62. Han, M., Vestal, C.R. & Zhang, Z.J. Quantum Couplings and Magnetic Properties of CoCr x Fe 2- x O 4 (0 < x < 1) Spinel Ferrite Nanoparticles Synthesized with Reverse Micelle Method. *The Journal of Physical Chemistry B* **108**, 583-587(2004).

63. White, R.J. et al. Supported metal nanoparticles on porous materials. Methods and applications. *Chemical Society reviews* **38**, 481-94(2009).

64. Yashima, M. et al. Structure and catalytic properties of nanosized alumina supported platinum and palladium particles synthesized by reaction in microemulsion. *Journal of Colloid and Interface Science* **268**, 348-356(2003).

65. Brunauer, S. & Emmett, P. Adsorption of Gases in Multimolecular Layers. *Journal of the American Chemical Society* **407**, (1938).

66. Carenco, S. et al. Controlled Design of Size-Tunable Monodisperse Nickel Nanoparticles. *Chemistry of Materials* **22**, 1340-1349(2010).

# APPENDICES

## Appendix A

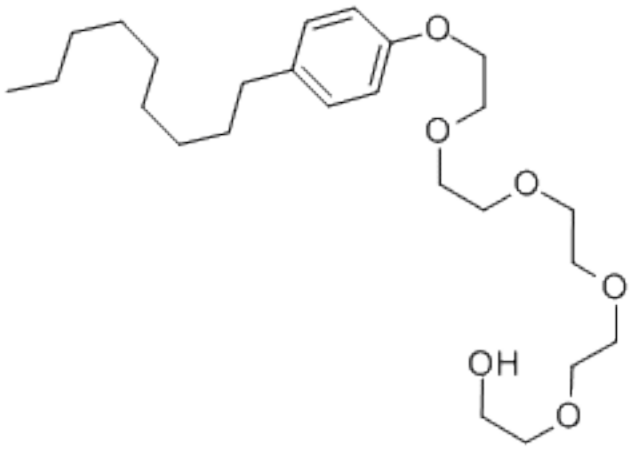


**Figure A.1** Molecular structure of IGEPAL CO-520 (NP5, polyoxyethylene nonylphenyl ether).

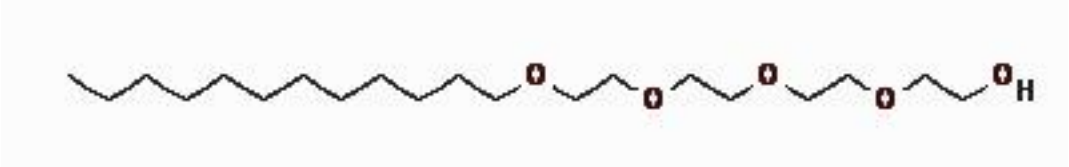


**Figure A.2.** Molecular structure of BRIJ-30 (tetraethylene glycol dodecyl ether).

Appendix B

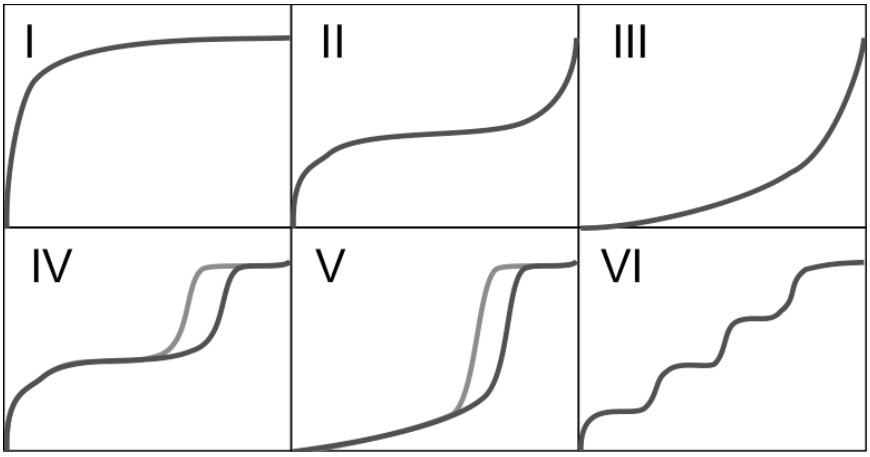


**Figure B.1.** IUPAC classification for adsorption Isotherms. I) Microporous solids. Chemisorption region. II & III) Macroporous adsorbents and finely divided non-porous solids. IV & V) Adsorption isotherms plots with hysteresis loops. Mesoporous materials characteristic plot. VI) Stepped isothermal plot for special cases.

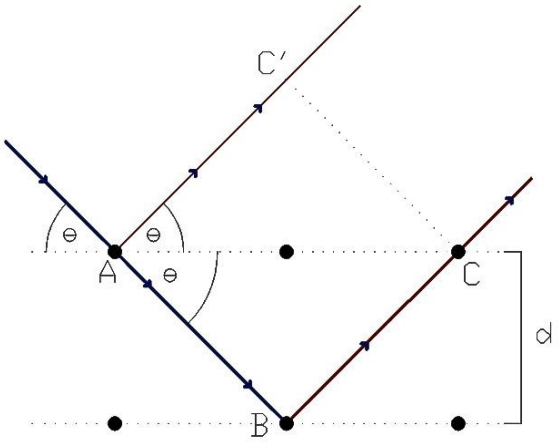


**Figure B.2.** Schematic representing Bragg's Law. Derivation from the figure is as follows:

$$n\lambda = AB + BC$$

$$AB = BC$$

$$\therefore n\lambda = 2AB$$

$$n\lambda = 2dsin\theta$$

# Appendix C

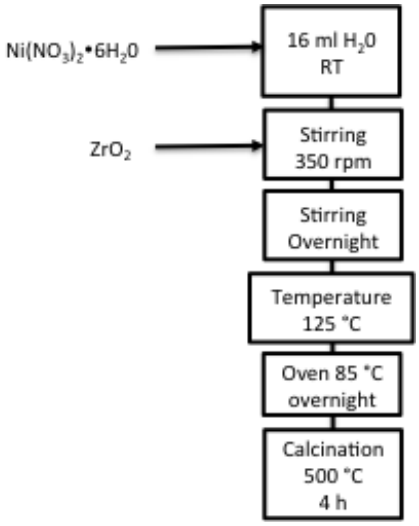


**Figure C.1.** Flow diagram of the synthetic procedure followed for obtaining catalyst using wet impregnation technique.

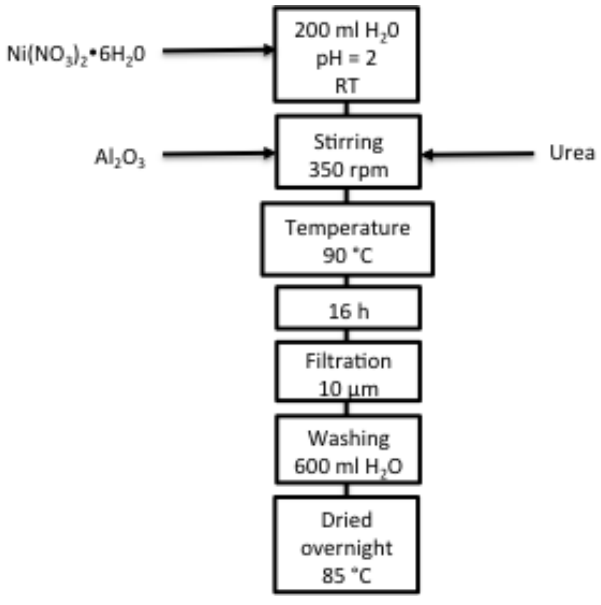


**Figure C.2.** Flow diagram of the synthetic procedure followed for obtaining catalyst using homogeneous deposition-precipitation technique.

# Appendix D

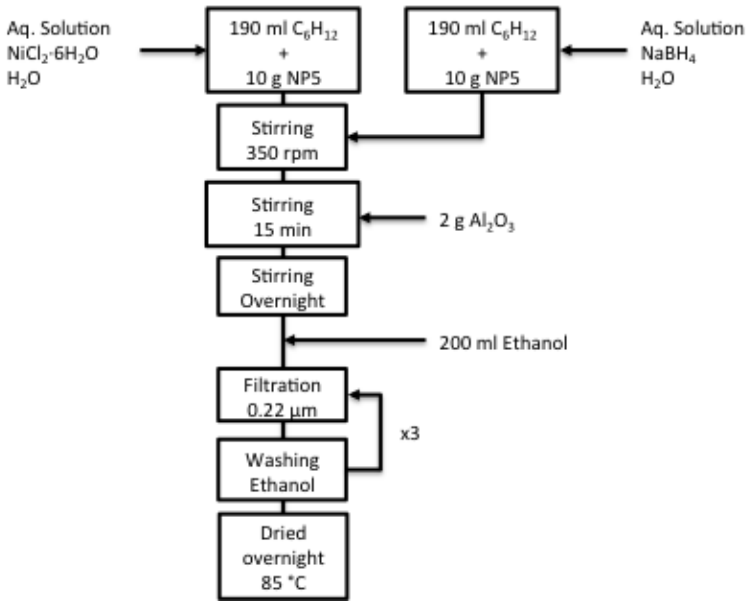


**Figure D.1.** Schematic synthesis procedure for supported nickel nanoparticles via microemulsion route. For this specific experiment Alumina is utilized as support. The concentration of nickel depends on the required metal loading in the support; the reducing agent concentration will correspond to 10 times the molar ratio of the metal. The water content in the MEM is determined by *w* parameter, depending on the desired particle size.

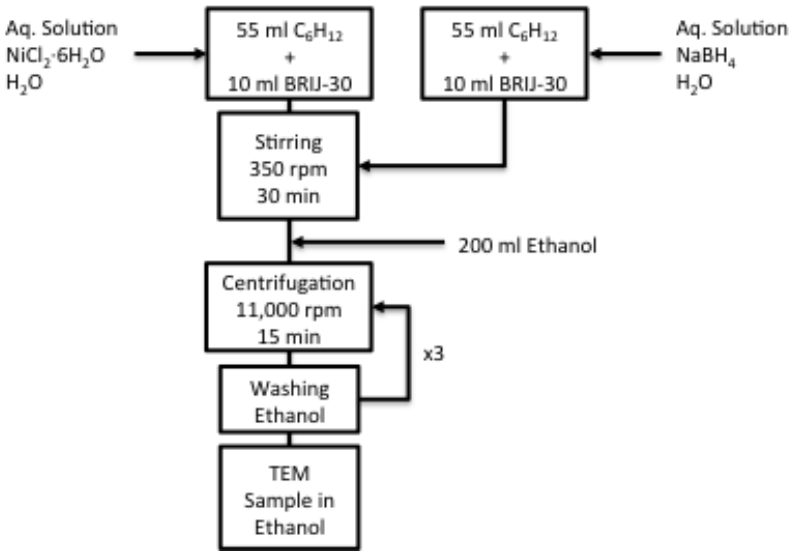


**Figure D.2.** Schematic synthesis of nickel nanoparticles via microemulsion for direct TEM characterization of the particle size. The water volume is calculated from the required *w*.

Appendix D

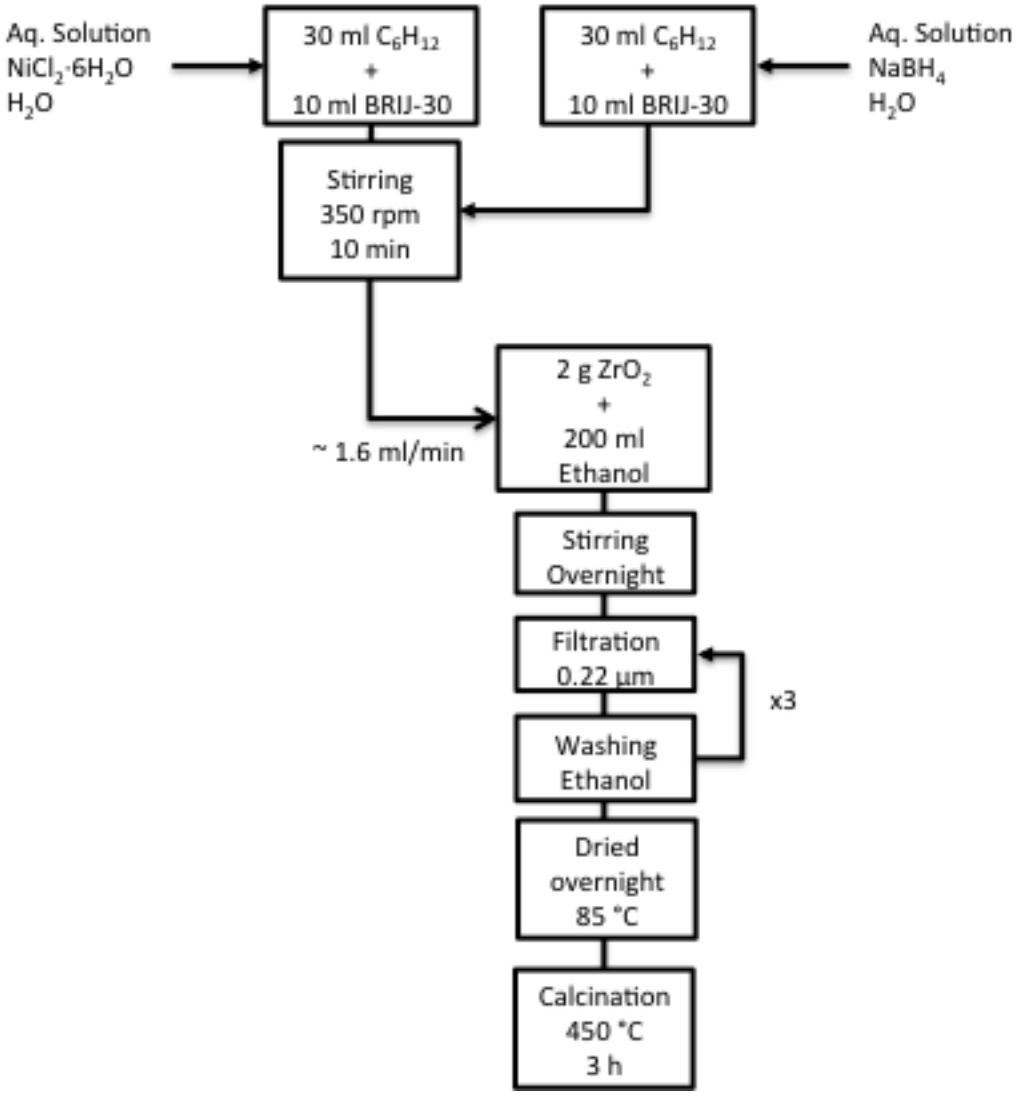


**Figure D.3.** Flow diagram representing the synthesis method for obtaining transition metal nanoparticles supported on zirconia. The concentration of the metal depends upon the desired loading of the sample. The water volume is calculated from the required *w* in respect of desired particle size. The reducing agent molar concentration is calculated from 1:10 molar ratio between the metal and $NaBH_4$ respectively.

# Appendix E

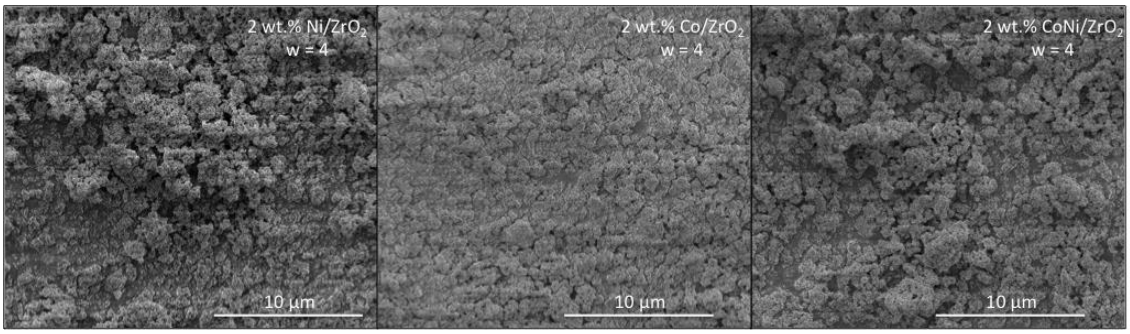


**Figure E.1.** SEM images obtained from samples prepared following the microemulsion method. From left to right; nickel, cobalt and cobalt-nickel nan0particles supported on zirconia.

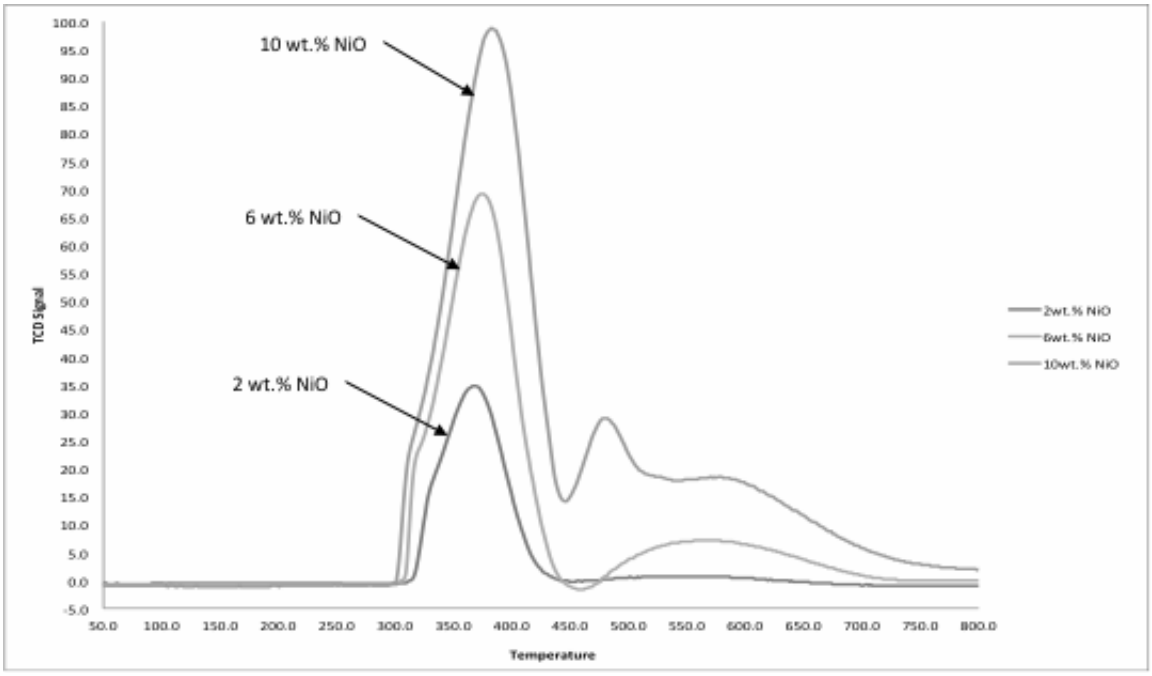


**Figure E.2.** TPR profiles of the reference samples prepared by physical mixture of commercially obtained NiO and zirconia.

# Appendix E

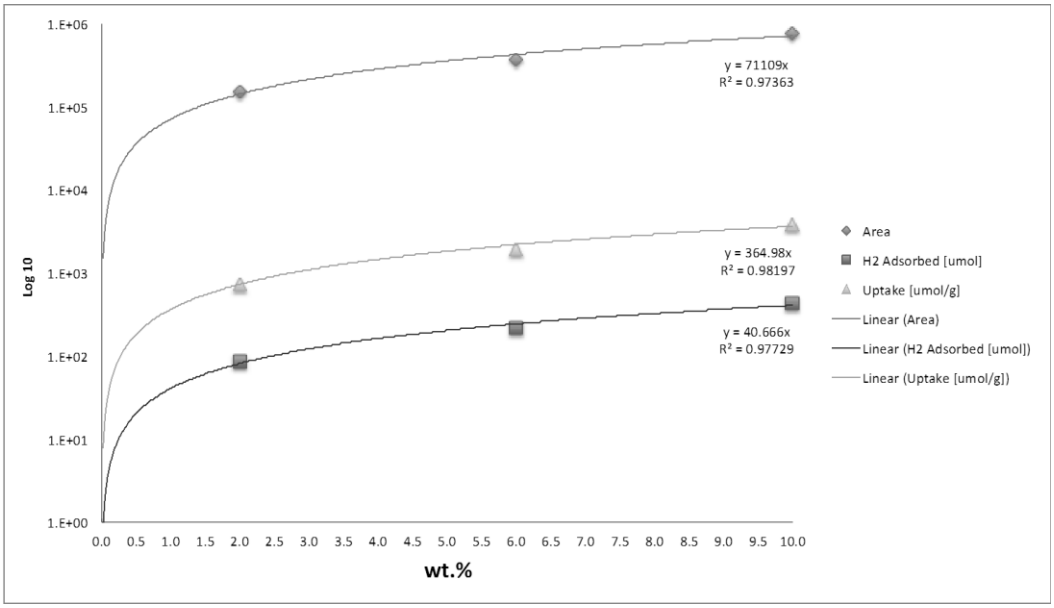


**Figure E.3.** The Inset represent the equation curves calculated from the area obtained in the experiments. From the Area of the curves in Figure F.2 the H2 uptake can be correlated and finally

Appendix F

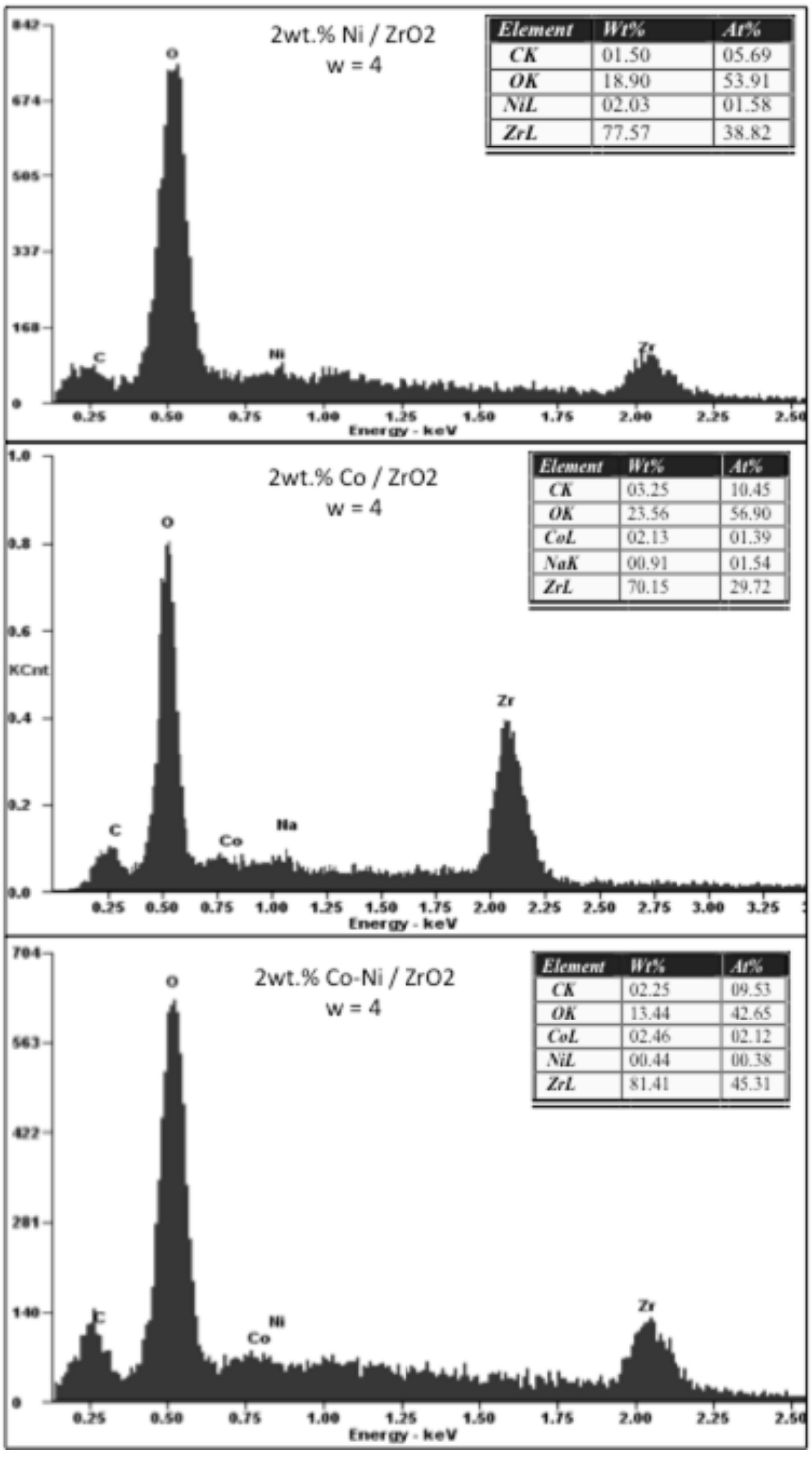


**Figure F.1.** Energy dispersive X-ray analysis (EDX) of the samples prepared via microemulsion with 0.87 M surfactant concentration. The elemental energy mapping indicates the presence of the specific elements in the samples. The inset on each section is a mathematical quantification of the intensity of the peak once an approximation curve is fit into the distribution of the peaks. It represents only a rough estimation of the expected weight percentage of each element in the sample.

Appendix F

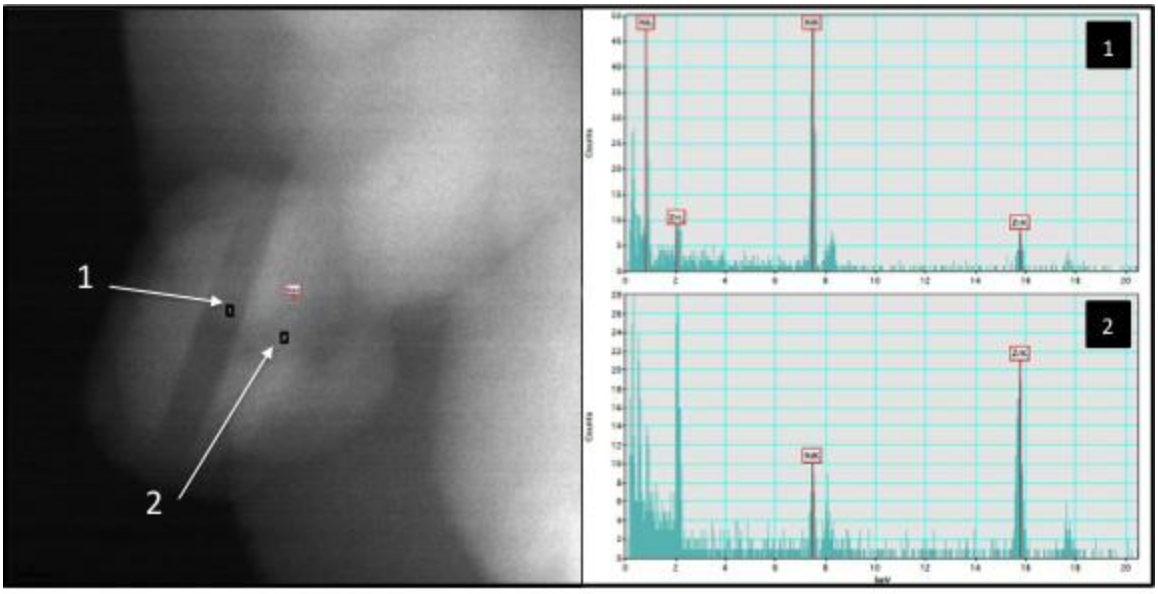


**Figure F.2.** Energy dispersive X-ray analysis (EDX) obtained from specific points in the generated HAADF STEM image from the right. During TEM analysis of the microemulsion samples EDS is performed in order to confirm the elemental composition of the particles observed. The image is taken from a representative 2wt.% $Ni/ZrO_2$ sample with $w$ = 4. Sample was Synthesized with 0.87 M surfactant concentration in the MEM system. Nickel and Zirconia energy peaks are highlighted on the right of the figure.

Appendix G

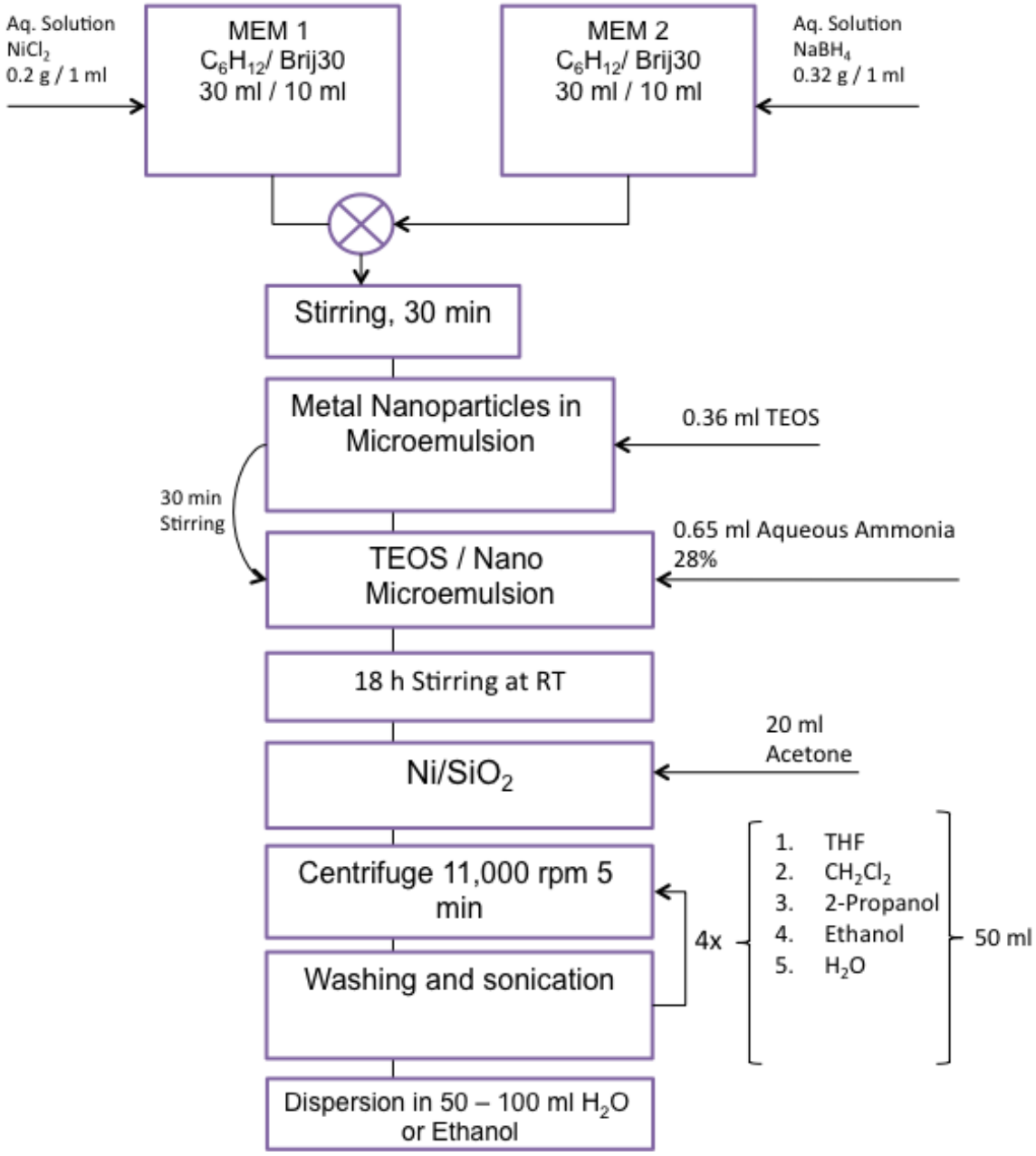


**Figure G.1.** Flow diagram of the synthesis process developed for one-step synthesis of supported size-controlled metal nanoparticles.